Variable kinematic shell elements for the analysis of electro-mechanical problems

Variable Kinematic Shell Elements for the Analysis of Electro-Mechanical Problems

Maria Cinefra*, Erasmo Carrera†‡, Stefano Valvano§
Aerospace Department, Politecnico di Torino, Italy

Keywords:
Shells, Finite Element Method, piezoelectric materials, Mixed Interpolated Tensorial Components, Carrera's Unified Formulation, layer-wise, laminated composites.

Author and address for Correspondence
Dr. Maria Cinefra
Research Assistant,
Department of Aeronautics and Space Engineering
Politecnico di Torino,
Corso Duca degli Abruzzi, 24,
10129 Torino, ITALY,
tel +39.011.546.6869, fax +39.011.564.6899
e.mail: maria.cinefra@polito.it

*Research Assistant, Aerospace Department, Politecnico di Torino, Corso Duca degli Abruzzi, 24, 10129 Torino, Italy, e-mail: maria.cinefra@polito.it, website: www.mul2.com.

†Professor, Aerospace Department, Politecnico di Torino, Corso Duca degli Abruzzi, 24, 10129 Torino, Italy, e-mail: erasmo.carrera@polito.it, website: www.mul2.com.

‡Department of Mathematics, Faculty of Science, King Abdulaziz University, P.O. Box 80203, Jeddah 21589, Saudi Arabia.

§PhD Student, Aerospace Department, Politecnico di Torino, Corso Duca degli Abruzzi, 24, 10129 Torino, Italy, e-mail: stefano.valvano@polito.it, website: www.mul2.com.

Abstract

The present paper considers the linear static analysis of both composite plate and shell structures embedding piezoelectric layers by means of a shell finite element with variable through-the-thickness kinematic. The refined models used are grouped in the Unified Formulation by Carrera (CUF) and they permit to accurately describe the distribution of displacements and stresses along the thickness of the multilayered shell. The shell element has nine nodes and the Mixed Interpolation of Tensorial Components (MITC) method is employed to contrast the membrane and shear locking phenomenon. The governing equations are derived from the Principle of Virtual Displacement (PVD) and the Finite Element Method (FEM) is employed to solve them. Cross-ply multilayered plates and cylindrical shells embedding piezoelectric layers are analysed, with simply-supported boundary conditions and subjected to sensor and actuator configurations. Various thickness ratios are considered. The results, obtained with different theories contained in the CUF, are compared with both the elasticity solutions given in literature and the analytical solutions obtained using the CUF and the Navier's method. From the analysis, one can conclude that the shell element based on the CUF is very efficient and its use is mandatory with respect to the classical models in the study of multilayered strcutures embedding piezo-layers.

1 Introduction

Piezoelectric materials have the ability to convert mechanical energy into electrical energy, and vice versa. For the last 50 years, the use of piezoelectric components as electro-mechanical transducers in sensor as well as in actuator applications has been continuously increasing. More recently, piezoelectrics have been considered among the most suitable materials for extending the structural capabilities beyond the purely passive load carrying one. Vibration and noise suppression, controlled active deformation and health monitoring are among the most important applications of these "intelligent" structural components. Analytical solution for general smart structural problems is a very difficult task and they exist, only, for a very few specialized and idealized cases. Meanwhile, the finite element method has become the most widely used technique to model various physical processes, including piezoelectricity. The introduction of piezoelectric material into a passive structure naturally leads to a multilayered component, and it has been recognized that classical models are not suitable for an accurate design of such structures, see for example the review article of Noor and Burton [1] and the references cited herein. Interlaminar Continuity (IC) of the transverse stresses as well as the related discontinuity of the slopes of the displacement distributions in thickness direction at the layers interfaces are the main effects arising in multilayered structures which can not be captured by classical formulations based on Love First Approximation Theories (LFAT), see e.g. [2]. Many refined theories for plates and shells have been proposed in order to meet the modeling requirements - known as C_z^0-Requirements - posed by these characteristics; further details can be found e.g. in the monograph of Reddy [3] and in the paper of Carrera [4]. For curved structures, Koiter [5] recognized the importance of transverse stress effects even for homogeneous shells and recommended the inclusion of such effects whenever a consistent higher-order model has to be proposed. The fundamentals for the modeling of piezoelectric materials have been given in many contributions, in particular in the pioneering works of Mindlin [6], EerNisse [7], Tiersten and Mindlin [8], and in the monograph of Tiersten [9]. The embedding of piezoelectric layers into plates and shells sharpens the requirements of an accurate modeling of the resulting adaptive structure due to the localized electro-mechanical coupling, see e.g. the review of Saravanos and Heyliger [10]. Therefore, within the framework of two-dimensional approaches, layerwise descriptions have been often proposed either for the electric field only (see e.g. the works of Kapuria [11] and of Ossadzow-David and Touratier [12]) or for both the mechanical and electrical unknowns (e.g. Heyliger et al. [13]). Ballhause et al. [14] showed that a fourth order assumption for the displacements leads to the correct closed form solution. They conclude that the analysis of local responses requires at least a layer-wise descriptions of the displacements, see also [15]. Benjeddou et al. [16] emphasized that a quadratic

electric potential through the plate thickness satisfies the electric charge conservation law exactly. An attempt to mathematically substantiate axiomatic two-dimensional piezoelectric shell formulations by the means of asymptotic expansions can be found in the book of Rogacheva [17]. An exhaustive overview of the many different modeling approaches and solution techniques for laminated piezoelectric plates and shells is far beyond the scope of this paper; more details on this topic can be found e.g. in the already cited review of Saravanos and Heyliger, and in the surveys of Gopinathan et al. [18] and of Benjeddou [19]. For the last years interest has been emerging for mixed formulations involving also stresses and dielectric displacements as primary variables, see for example the recent works of Lammering et al. [20] and of Benjeddou et al. [21]. Some of the latest contributions to the Finite Elements (FEs) analysis of piezoelectric plates that includes an FSDT description of displacements and a layer-wise (LW) form of the electric potential was developed by Sheik et al. [22]. The numerical, membrane and bending behavior of FEs that are based on FSDTs were analyzed by Auricchio et al. [23] in the framework of a suitable variational formulation. The third-order theory of HOT type was applied by Thornburg and Chattopadhyay [24] to derive FEs that take into consideration the electro-mechanical coupling. Similar elements have more recently been considered by Shu [25]. The extension of the third-order zig-zag Ambartsumian multilayered theory to finite analysis of electro-mechanical problems has been proposed by Oh and Cho [26]. An extension to piezoelectricity of numerically efficient plate/shell elements based on the mixed interpolation of tensorial components formulation has recently been provided by Kogl and Bucalem [27],[28]. Some of the latest contributions to the Finite Elements (FEs) analysis of piezoelectric shells that are based on exact geometry solid-shell element with the first-order 7-parameter equivalente single layer theory was developed by Kulikov et al. [29], and a piezoelectric solid shell element with a mixed variational formulation and a geometrically nonlinear theory was developed by Klinkel et al. [30]. A new shell finite element is presented in this paper for the analysis of composite structures with piezo-layers. It is based on the Carrera's Unified Formulation (CUF), which has been developed by Carrera for multi-layered structures [31]. Many works have been devoted to the extension of the CUF. Among others, Carrera [32] extends PVD and RMVT variational statements to piezo-laminated plates. The modeling of piezo-laminated plates using LW mixed FEs was then proposed in [33]. Subsequently, an extension of the RMVT to piezoelectric laminates with analytical results was published in [34]. Mixed FEs for static and dynamics analysis of piezo-electric plates have been provided in [35], where only transverse stresses were modeled by RMVT. Mixed FEs with direct evaluation of transverse electric displacement have been provided in [36]. Layer Wise (LW) theories contained in the CUF have been implemented in the present shell finite element. An analytical solution type has already been successfully employed in combination with the Unified Formulation for piezoelectric plates [14] and piezoelectric shells [15]. The cylindrical geometry is considered and the Mixed Interpolation of Tensorial Components (MITC) method [37]-[38] is used to contrast the membrane and shear locking. The governing equations for the static analysis of composite structures are derived from the Principle of Virtual Displacement (PVD), in order to apply the finite element method. Some composite cylindrical shells are analyzed and the results, obtained with the different models contained in the CUF, are compared with the analytical solution and the exact solution given in literature.

2 Unified Formulation

The main feature of the Unified Formulation by Carrera [32],[39],[40] (CUF) is the unified manner in which the displacement variables are handled. According to CUF, the displacement field and the potential field are written by means of approximating functions in the thickness direction as follows:

$$\boldsymbol{u}^k(\alpha,\beta,z) = F_\tau(z)\boldsymbol{u}^k_\tau(\alpha,\beta)\ , \quad \delta\boldsymbol{u}^k(\alpha,\beta,z) = F_s(z)\delta\boldsymbol{u}^k_s(\alpha,\beta)\ , \quad \tau,s = 0,1,...,N\,, \tag{1}$$

$$\Phi^k(\alpha,\beta,z) = F_\tau(z)\Phi^k_\tau(\alpha,\beta)\ , \quad \delta\Phi^k(\alpha,\beta,z) = F_s(z)\delta\Phi^k_s(\alpha,\beta)\ , \quad \tau,s = 0,1,...,N\ , \tag{2}$$

where (α,β,z) is a curvilinear coordinates reference system, defined in the next section, and the displacement $\boldsymbol{u} = \{u,v,w\}$ and the potential $\boldsymbol{\Phi}$ are referred to such system. δ indicates the virtual variation and k identifies the layer. F_τ and F_s are the so-called thickness functions depending only on z. $\boldsymbol{u}_s$ and Φ_s are the unknown variables depending on the coordinates α and β. τ and s are sum indexes and N is the order of expansion in the thickness direction assumed for the variables.

In the case of Layer-Wise (LW) models, the displacement and the potential are defined at k-layer level:

$$\boldsymbol{u}^k = F_t\,\boldsymbol{u}^k_t + F_b\,\boldsymbol{u}^k_b + F_r\,\boldsymbol{u}^k_r = F_\tau\,\boldsymbol{u}^k_\tau, \qquad \tau = t,b,r\ , \quad r = 2,...,N. \tag{3}$$

$$\Phi^k = F_t\,\Phi^k_t + F_b\,\Phi^k_b + F_r\,\Phi^k_r = F_\tau\,\Phi^k_\tau, \qquad \tau = t,b,r\ , \quad r = 2,...,N. \tag{4}$$

$$F_t = \frac{P_0+P_1}{2}, \quad F_b = \frac{P_0-P_1}{2}, \quad F_r = P_r - P_{r-2}. \tag{5}$$

The top (t) and bottom (b) values of the displacements and the potential are used as unknown variables and one can impose the following compatibility conditions:

$$u^k_t = u^{k+1}_b, \qquad \Phi^k_t = \Phi^{k+1}_b, \qquad k = 1, N_l - 1. \tag{6}$$

The LW models, in respect to the Equivalent Single Layer models (ESL), allow the zig-zag form of the variables distribution in layered structures to be modelled.

3 MITC9 shell element

In this section, the derivation of a shell finite element for the analysis of multilayered structures is presented. The element is based LW theories contained in the Unified Formulation. A nine-nodes shell element is considered. After an overview in scientific literature about the methods that permit to withstand the membrane and shear locking, the MITC technique has been adopted for this element.

3.1 Shell geometry

Shells are bi-dimensional structures in which one dimension (in general the thickness in z direction) is negligible with respect to the other two in-plane dimensions. Geometry and the reference system are indicated in Fig. 2. By considering multilayered structures, the square of an infinitesimal linear segment in the layer, the associated infinitesimal area and volume are given by:

$$\begin{aligned} ds^2_k &= H^{k\,2}_\alpha\, d\alpha^2_k + H^{k\,2}_\beta\, d\beta^2_k + H^{k\,2}_z\, dz^2_k\ , \\ d\Omega_k &= H^k_\alpha H^k_\beta\, d\alpha_k\, d\beta_k\ , \\ dV &= H^k_\alpha\, H^k_\beta\, H^k_z\, d\alpha_k\, d\beta_k\, dz_k\ , \end{aligned} \tag{7}$$

where the metric coefficients are:

$$H^k_\alpha = A^k(1 + z_k/R^k_\alpha), \quad H^k_\beta = B^k(1 + z_k/R^k_\beta), \quad H^k_z = 1\ . \tag{8}$$

k denotes the k-layer of the multilayered shell; R^k_α and R^k_β are the principal radii of the midsurface of the layer k. A^k and B^k are the coefficients of the first fundamental form of Ω_k (Γ_k is the Ω_k boundary). In this paper, the attention has been restricted to shells with constant radii of curvature (cylindrical,

spherical, toroidal geometries) for which $A^k = B^k = 1$, in particular cylindrical shells have been considered. Details for shells are reported in [17].

Geometrical relations can be expressed in matrix form as:

$$\begin{aligned} \boldsymbol{\epsilon}_p =& [\epsilon_{\alpha\alpha}, \epsilon_{\beta\beta}, \epsilon_{\alpha\beta}] = (\boldsymbol{D}_p + \boldsymbol{A}_p)\boldsymbol{u}\,, \\ \boldsymbol{\epsilon}_n =& [\epsilon_{\alpha z}, \epsilon_{\beta z}, \epsilon_{zz}] = (\boldsymbol{D}_{np} + \boldsymbol{D}_{nz} - \boldsymbol{A}_n)\boldsymbol{u}\,, \end{aligned} \tag{9}$$

Where the differential operators are defined as follows:

$$\boldsymbol{D}_p = \begin{bmatrix} \frac{\partial_\alpha}{H_\alpha} & 0 & 0 \\ 0 & \frac{\partial_\beta}{H_\beta} & 0 \\ \frac{\partial_\beta}{H_\beta} & \frac{\partial_\alpha}{H_\alpha} & 0 \end{bmatrix} \quad , \quad \boldsymbol{D}_{np} = \begin{bmatrix} 0 & 0 & \frac{\partial_\alpha}{H_\alpha} \\ 0 & 0 & \frac{\partial_\beta}{H_\beta} \\ 0 & 0 & 0 \end{bmatrix} \quad , \quad \boldsymbol{D}_{nz} = \begin{bmatrix} \partial_z & 0 & 0 \\ 0 & \partial_z & 0 \\ 0 & 0 & \partial_z \end{bmatrix} \tag{10}$$

$$\boldsymbol{A}_p = \begin{bmatrix} 0 & 0 & \frac{1}{H_\alpha R_\alpha} \\ 0 & 0 & \frac{1}{H_\beta R_\beta} \\ 0 & 0 & 0 \end{bmatrix} \,, \boldsymbol{A}_n = \begin{bmatrix} \frac{1}{H_\alpha R_\alpha} & 0 & 0 \\ 0 & \frac{1}{H_\beta R_\beta} & 0 \\ 0 & 0 & 0 \end{bmatrix} \tag{11}$$

The geometrical relations between electric field $\mathcal{E}$ and potential Φ are defined as follows:

$$\begin{aligned} \boldsymbol{\mathcal{E}}_p &= [\mathcal{E}_\alpha, \mathcal{E}_\beta]^T = -\boldsymbol{D}_{ep}\, \Phi\,, \\ \boldsymbol{\mathcal{E}}_n &= [\mathcal{E}_z]^T = -\boldsymbol{D}_{en}\, \Phi\,, \end{aligned} \tag{12}$$

Where the differential operators are defined as follows:

$$\boldsymbol{D}_{ep} = \begin{bmatrix} \frac{\partial_\alpha}{H_\alpha} \\ \frac{\partial_\beta}{H_\beta} \end{bmatrix} \quad , \quad \boldsymbol{D}_{en} = \begin{bmatrix} \partial_z \end{bmatrix} \ .$$

3.2 MITC method

A shell finite element is here presented for the analysis of composite structures. It is based on the Carrera's Unified Formulation (CUF), which was developed by Carrera for multi-layered structures [31].

According to the finite element method, the displacement and the potential components are interpolated on the nodes of the element by means of the Lagrangian shape functions N_i:

$$\delta \boldsymbol{u}_s = N_i \delta \boldsymbol{q}_{u s_i} \qquad \boldsymbol{u}_\tau = N_j \boldsymbol{q}_{u \tau_j} \qquad \text{with} \quad i, j = 1, ..., 9 \tag{13}$$

$$\delta \Phi_s = N_i \delta q_{\Phi s_i} \qquad \Phi_\tau = N_j q_{\Phi \tau_j} \qquad \text{with} \quad i, j = 1, ..., 9 \tag{14}$$

where $\boldsymbol{q}_{u\tau_j} = (q_{u_\tau}, q_{v_\tau}, q_{w_\tau})$ and $\delta \boldsymbol{q}_{u s_i} = (\delta q_{u_s}, \delta q_{v_s}, \delta q_{w_s})$ are the nodal displacements and their virtual variations for the mechanical variables, and $q_{\Phi\tau_j} = (q_{\Phi_\tau})$ and $\delta q_{\Phi s_i} = (\delta q_{\Phi_s})$ are the nodal potential and their virtual variation for the electric variable. Substituting in the geometrical relations (9) one has:

$$\begin{aligned}\boldsymbol{\epsilon}_p =& F_\tau(\boldsymbol{D}_p + \boldsymbol{A}_p)(N_i)\boldsymbol{q}_{\tau_i} \\ \boldsymbol{\epsilon}_n =& F_\tau(\boldsymbol{D}_{n\Omega} - \boldsymbol{A}_n)(N_i)\boldsymbol{q}_{\tau_i} + F_{\tau,3}\boldsymbol{A}_{nz}(N_i)\boldsymbol{q}_{\tau_i}\end{aligned} \tag{15}$$

Considering the local coordinate system (ξ, η), the MITC shell elements ([41],[42]) are formulated by using, instead of the strain components directly computed from the displacements, an interpolation of these within each element using a specific interpolation strategy for each component. The corresponding interpolation points, called tying points, are shown in Fig. 3 for the MITC9 shell element.
The interpolating functions are lagrangian and are calculated by imposing that the function assumes the value 1 in the corresponding tying point and 0 in the others. These are arranged in the following arrays:

$$\begin{aligned}N_{m1} &= [N_{A1}, N_{B1}, N_{C1}, N_{D1}, N_{E1}, N_{F1}] \\ N_{m2} &= [N_{A2}, N_{B2}, N_{C2}, N_{D2}, N_{E2}, N_{F2}] \\ N_{m3} &= [N_P, N_Q, N_R, N_S]\end{aligned} \tag{16}$$

From this point on, the subscripts $m1$, $m2$ and $m3$ indicate quantities calculated in the points $(A1, B1, C1, D1, E1, F1)$, $(A2, B2, C2, D2, E2, F2)$ and (P, Q, R, S), respectively. Therefore, the strain components are interpolated as follows:

$$\begin{aligned}\boldsymbol{\epsilon}_p &= \begin{bmatrix}\epsilon_{\alpha\alpha} \\ \epsilon_{\beta\beta} \\ \epsilon_{\alpha\beta}\end{bmatrix} = \begin{bmatrix}N_{m1} & 0 & 0 \\ 0 & N_{m2} & 0 \\ 0 & 0 & N_{m3}\end{bmatrix} \begin{bmatrix}\epsilon_{\alpha\alpha_{m1}} \\ \epsilon_{\beta\beta_{m2}} \\ \epsilon_{\alpha\beta_{m3}}\end{bmatrix} \\ \boldsymbol{\epsilon}_n &= \begin{bmatrix}\epsilon_{\alpha z} \\ \epsilon_{\beta z} \\ \epsilon_{zz}\end{bmatrix} = \begin{bmatrix}N_{m1} & 0 & 0 \\ 0 & N_{m2} & 0 \\ 0 & 0 & 1\end{bmatrix} \begin{bmatrix}\epsilon_{\alpha z_{m1}} \\ \epsilon_{\beta z_{m2}} \\ \epsilon_{zz}\end{bmatrix}\end{aligned} \tag{17}$$

where the strains $\epsilon_{\alpha\alpha_{m1}}$, $\epsilon_{\beta\beta_{m2}}$, $\epsilon_{\alpha\beta_{m3}}$, $\epsilon_{\alpha z_{m1}}$, $\epsilon_{\beta z_{m2}}$ are expressed by means of eq.s (15) and the shape functions N_i are calculated in the tying points.

4 Constitutive equations

The second step towards the governing equations is the definition of the constitutive equations that permit the stresses and the electric displacements to be expressed by means of the strains and the electric fields. The generalized Hooke's law is considered, by employing a linear constitutive model for infinitesimal deformations. A linear coupling of the electric fields is employed to complete stresses equations and to describe the electric displacements equations. In a composite material, these equations are obtained in material coordinates $(1, 2, 3)$ for each layer k and then rotated in the general curvilinear reference system (α, β, z).

Therefore, the in-plane stresses $\boldsymbol{\sigma}_p = [\sigma_{\alpha\alpha}, \sigma_{\beta\beta}, \sigma_{\alpha\beta}]$, the transverse stresses $\boldsymbol{\sigma}_n = [\sigma_{\alpha z}, \sigma_{\beta z}, \sigma_{zz}]$ and the electric displacements $\boldsymbol{\mathcal{D}} = [\mathcal{D}_\alpha, \mathcal{D}_\beta, \mathcal{D}_z]$ after the rotation are:

$$\boldsymbol{\sigma}^k_{pC} = \boldsymbol{C}^k_{pp}\boldsymbol{\epsilon}^k_{pG} + \boldsymbol{C}^k_{pn}\boldsymbol{\epsilon}^k_{nG} - \boldsymbol{e}^{k^T}_{pp}\boldsymbol{\mathcal{E}}^k_{pG} - \boldsymbol{e}^{k^T}_{np}\boldsymbol{\mathcal{E}}^k_{nG} \tag{18}$$

$$\boldsymbol{\sigma}^k_{nC} = \boldsymbol{C}^k_{np}\boldsymbol{\epsilon}^k_{pG} + \boldsymbol{C}^k_{nn}\boldsymbol{\epsilon}^k_{nG} - \boldsymbol{e}^{k^T}_{pn}\boldsymbol{\mathcal{E}}^k_{pG} - \boldsymbol{e}^{k^T}_{nn}\boldsymbol{\mathcal{E}}^k_{nG} \tag{19}$$

$$\boldsymbol{\mathcal{D}}^k_{pC} = \boldsymbol{e}^k_{pp}\boldsymbol{\epsilon}^k_{pG} + \boldsymbol{e}^k_{pn}\boldsymbol{\epsilon}^k_{nG} + \boldsymbol{\varepsilon}^k_{pp}\boldsymbol{\mathcal{E}}^k_{pG} + \boldsymbol{\varepsilon}^k_{pn}\boldsymbol{\mathcal{E}}^k_{nG} \tag{20}$$

$$\boldsymbol{\mathcal{D}}^k_{nC} = \boldsymbol{e}^k_{np}\boldsymbol{\epsilon}^k_{pG} + \boldsymbol{e}^k_{nn}\boldsymbol{\epsilon}^k_{nG} + \boldsymbol{\varepsilon}^k_{np}\boldsymbol{\mathcal{E}}^k_{pG} + \boldsymbol{\varepsilon}^k_{nn}\boldsymbol{\mathcal{E}}^k_{nG} \tag{21}$$

where

$$\begin{aligned}
\boldsymbol{C}^k_{pp} &= \begin{bmatrix} C^k_{11} & C^k_{12} & C^k_{16} \\ C^k_{12} & C^k_{22} & C^k_{26} \\ C^k_{16} & C^k_{26} & C^k_{66} \end{bmatrix} \qquad \boldsymbol{C}^k_{pn} = \begin{bmatrix} 0 & 0 & C^k_{13} \\ 0 & 0 & C^k_{23} \\ 0 & 0 & C^k_{36} \end{bmatrix} \\
\boldsymbol{C}^k_{np} &= \begin{bmatrix} 0 & 0 & 0 \\ 0 & 0 & 0 \\ C^k_{13} & C^k_{23} & C^k_{36} \end{bmatrix} \qquad \boldsymbol{C}^k_{nn} = \begin{bmatrix} C^k_{55} & C^k_{45} & 0 \\ C^k_{45} & C^k_{44} & 0 \\ 0 & 0 & C^k_{33} \end{bmatrix}
\end{aligned} \tag{22}$$

$$\begin{aligned}
\boldsymbol{e}_{pp} &= \begin{bmatrix} 0 & 0 & 0 \\ 0 & 0 & 0 \end{bmatrix} , \quad \boldsymbol{e}_{pn} = \begin{bmatrix} e_{15} & e_{14} & 0 \\ e_{25} & e_{24} & 0 \end{bmatrix} , \\
\boldsymbol{e}_{np} &= \begin{bmatrix} e_{31} & e_{32} & e_{36} \end{bmatrix} , \quad \boldsymbol{e}_{nn} = \begin{bmatrix} 0 & 0 & e_{33} \end{bmatrix} .
\end{aligned} \tag{23}$$

$$\begin{aligned}
\boldsymbol{\varepsilon}_{pp} &= \begin{bmatrix} \varepsilon_{11} & \varepsilon_{12} \\ \varepsilon_{12} & \varepsilon_{22} \end{bmatrix} , \quad \boldsymbol{\varepsilon}_{pn} = \begin{bmatrix} 0 \\ 0 \end{bmatrix} , \\
\boldsymbol{\varepsilon}_{np} &= \begin{bmatrix} 0 & 0 \end{bmatrix} , \quad \boldsymbol{\varepsilon}_{nn} = \begin{bmatrix} \varepsilon_{33} \end{bmatrix} .
\end{aligned} \tag{24}$$

The material coefficients C_{ij} depend on the Young's moduli E_1, E_2, E_3, the shear moduli G_{12}, G_{13}, G_{23} and Poisson moduli ν_{12}, ν_{13}, ν_{23}, ν_{21}, ν_{31}, ν_{32} that characterize the layer material. The piezoelectric material is characterized by the piezoelectric coefficients e_{ij} and the permittivity coefficients ε_{ij}.

5 Governing equations

This section presents the derivation of the governing finite element stiffness matrix based on the Principle of Virtual Displacement (PVD) in the case of multi-layered shell structures subjected to electromechanical loads. The PVD for a multilayered piezoelectric structure reads:

$$\int_V \left(\delta\boldsymbol{\epsilon}_{pG}{}^T \boldsymbol{\sigma}_{pC} + \delta\boldsymbol{\epsilon}_{nG}{}^T \boldsymbol{\sigma}_{nC} - \delta\boldsymbol{\mathcal{E}}_{pG}{}^T \boldsymbol{\mathcal{D}}_{pC} - \delta\boldsymbol{\mathcal{E}}_{nG}{}^T \boldsymbol{\mathcal{D}}_{nC} \right) dV = \delta L_e \tag{25}$$

where Ω_k and A_k are the integration domains in the plane and in the thickness direction. The first member of the equation represents the variation of the internal work, while the second member is the external work. In order to refer the integration domains to the midsurface of each layer in the curvilinear coordinate system, one has to introduce the parameters H_α , H_β as follows:

$$\int_{\Omega_k}\int_{A_k} \left\{ \delta\boldsymbol{\epsilon}^k_{pG}{}^T \boldsymbol{\sigma}^k_{pC} + \delta\boldsymbol{\epsilon}^k_{nG}{}^T \boldsymbol{\sigma}^k_{nC} - \delta\boldsymbol{\mathcal{E}}^k_{pG}{}^T \boldsymbol{\mathcal{D}}^k_{pC} - \delta\boldsymbol{\mathcal{E}}^k_{nG}{}^T \boldsymbol{\mathcal{D}}^k_{nC} \right\} H_\alpha H_\beta \, d\Omega_k dz = \delta L_e \tag{26}$$

Substituting the constitutive equations 18 - 21, the geometrical relations written via the MITC method 17 and applying the Unified Formulation 1 and the FEM approximation 13, one obtains the following governing equations:

$$\delta \boldsymbol{u}_s^k : \boldsymbol{K}_{uu}^{k\tau s} \boldsymbol{u}_\tau^k + \boldsymbol{K}_{u\Phi}^{k\tau s} \Phi_\tau^k = \boldsymbol{P}_{us}^k \tag{27}$$

$$\delta \boldsymbol{\Phi}_s^k : \boldsymbol{K}_{\Phi u}^{k\tau s} \boldsymbol{u}_\tau^k + \boldsymbol{K}_{\Phi\Phi}^{k\tau s} \Phi_\tau^k = \boldsymbol{P}_{\Phi s}^k \tag{28}$$

In compact form:

$$\delta \boldsymbol{q}_s^k \ : \ \boldsymbol{K}^{k\tau s} \, \boldsymbol{q}_\tau^k \ = \ \boldsymbol{P}_s^k \tag{29}$$

where

$$\boldsymbol{K}^{k\tau s} = \begin{bmatrix} \boldsymbol{K}_{uu} & \boldsymbol{K}_{u\Phi} \\ \boldsymbol{K}_{\Phi u} & \boldsymbol{K}_{\Phi\Phi} \end{bmatrix}^{k\tau s} \tag{30}$$

The mechanical part $\boldsymbol{K}_{uu}^{k\tau sij}$ is a 3×3 matrix, the coupling matrices $\boldsymbol{K}_{u\Phi}^{k\tau sij}$, $\boldsymbol{K}_{\Phi u}^{k\tau sij}$ have dimension 3×1 and 1×3 respectively, and the electrical part $\boldsymbol{K}_{\Phi\Phi}^{k\tau sij}$ is a 1×1 matrix. The global matrix $\boldsymbol{K}^{k\tau sij}$ is called fundamental nucleus, and its explicit expression is given in Appendix. This is the basic element from which the stiffness matrix of the whole structure is computed. For the expansion of the fundamental nucleus on the indexes τ and s and the assembling procedure at multi-layer level for LW approaches, the reader can refer to [32]. $\boldsymbol{q}_\tau^k = (q_{u_\tau}^k, q_{v_\tau}^k, q_{w_\tau}^k, q_{\Phi_\tau}^k)$ is the vector of the nodal mechanical displacements and the nodal electric potential. $\boldsymbol{P}_s^k$ is the fundamental nucleus for the external load.

6 Numerical results and discussion

The model introduced, unlike 3-D degenerate approach, does not involve an approximation of the geometry of the shell and it describes accurately the curvature of the shell. However, the locking phenomenon is still present. In this work, such a model is combined with a simple displacement formulation for the analysis of composite structures. The refined theories contained in CUF, coupled with the MITC method, permit to increase the degree of approximation by increasing the order of expansion of displacements in the thickness direction and the number of used elements. In electro-mechanical problems it is necessary to impose the value of the electric potential variable at top and bottom position. To obtain this, Layer-Wise models with Legendre polynomials are employed. The efficiency of Layer-Wise models is tested with the finite element scheme, and the numerical results are compared with the ones obtained with the 3D elasticity approach. In this direction, two kind of reference problems are considered: the composite square plate embedding piezoelectric layers at top and bottom position, analytically analyzed by Carrera [14], and single and multilayered cylinders embedding piezoelectric layers, analytically analyzed. Both of them are evaluated in sensor and actuator configuration. For the sensor case, a bi-sinusoidal transverse normal pressure is applied at the top surface for the plate and at the bottom surface for the shells:

$$p_z^{\pm} = \hat{p}_z^{\pm} \, sin(m\pi\alpha/a) sin(n\pi\beta/b) \tag{31}$$

with amplitude $\hat{p}_z^{\pm} = 1$ and wave numbers $m = 1$, $n = 1$ for the plate and $n = 8$ for the shell. The potential at top and bottom position is imposed $\Phi_t = \Phi_b = 0$.

For the actuator case, a bi-sinusoidal electric potential is imposed at top surface:

$$\Phi^{+} = \hat{\phi}_z^{+} \, sin(m\pi\alpha/a) sin(n\pi\beta/b) \tag{32}$$

with amplitude $\hat{\phi}_z^{+} = 1$ and wave numbers $m = 1$, $n = 1$ for the plate and $n = 8$ for the shell. The potential at bottom position is imposed $\Phi_b = 0$. No mechanical load is applied.

The two problems are briefly described in the following sections. In this paper some acronyms are used in tables and figures. The first letter indicates the multi-layer approach, Layer Wise (L). The second letter refers to the employed variational statement: in this work only the Principle of Virtual Displacements D is used. Only for the multilayered shell, reference solutions are calculated with Full Reissner Mixed Variational Theory, so the second letters are FM. The number N indicates the order of expansion used in the thickness direction (from 1 to 4). For references solutions obtained with analytical method a subscript a is used.

6.1 Multilayered plate

The structure analyzed by Carrera [14] (see Figure 1) is a composite square plate embedding piezoelectric layers made globally of four layers, a core in Gr/Ep composite material by two orthotropic layers with lamination (0°/90°), and the skins in PZT-4 by two piezoelectric layers. In respect to the total thickness, a single piezoelectric skin is thick $h_p = 0.1h_{tot}$, while the single core layer is thick $h_c = 0.4h_{tot}$. The physical properties of the shell are given in Table 1.

Due to the symmetry of both the geometry and the load, a quarter of plate is analysed and the following symmetry and boundary conditions (simply-supported) are applied:

$$\begin{aligned} u_\tau(0, y) &= 0 \\ v_\tau(x, 0) &= 0 \\ w_\tau(x, b/2) &= 0 \\ w_\tau(a/2, y) &= 0 \\ u_\tau(x, b/2) &= 0 \\ v_\tau(a/2, y) &= 0 \end{aligned} \tag{33}$$

with $\tau = 0, 1, ..., N$.
The results are presented for different thickness ratios $a/h = 2, 4, 10, 100$.
A mesh grid of 12×12 elements is taken to ensure the convergence of the solution.

In general the results approach to the exact solution by increasing the order of expansion N for the various thickness ratios, see Tables 2, 4 . One can note that the element doesn't suffer the locking phenomenon even when the plate is very thin ($a/h = 100$), see Tables 3, 5. Only the LD4 model is able to exactly reproduce the analitycal solution in the case of thick shell. The behavior of shear and transverse stresses $\sigma_{\alpha z}$, σ_{zz} is non-linear along the thickness of the plate. The continuity conditions are reached only by increasing the order of expansion N, see Figures 5 - 11. Only for the actuator case of very thin plates ($a/h = 100$), the LD4 model is not able to fulfill the continuity conditions of transverse stresses σ_{zz} at the interfaces between layers, see Figures 12. To overcome this problem a mixed variational principle could be used. For the description of the electric potential Φ it is necessary to use the higher-order model, LD4, to describe the non-linear behavior in thick plates ($a/h = 2$), see Figures 13, 17. On the other hand for thin plates ($a/h = 100$) a layer-wise description of lower order is sufficient, see Figures 14, 18. The electric displacement $\mathcal{D}_z$ has a non-linear behavior for every thickness ratio in the sensor case, it is necessary an higher-order model to obtain the continuity interface, see Figures 15, 16. For the actuator case, due to its linear behavior, the electric displacement can be descripted by lower-order layer-wise model, see Figures 19, 20.

6.2 Multilayered piezoelectric cylinder.

The structure analyzed by Carrera [43] (see Figure 4) is a mono-layered piezoelectric cylinder, with the material properties given in Table 1. Moreover a 3 layer configuration cylinder with the core in Gr/Ep composite material is analysed. For multilayered cases, reference solutions are evaluated with an analytical Layer-Wise Full Mixed approach (LWFM). With the LWFM it is possible to impose the interface continuity of both mechanical transverse stresses and normal electric displacement variables.

The geometrical parameters of the considered cylinder are: $a = 40$, $b = 2\pi R_\beta$, $R_\beta = 10$.

Due to the symmetry of both the geometry and the load, an octave of the cylinder is studied (1/2 in the axial direction and 1/4 in the hoop direction). The following symmetry conditions are applied:

$$\begin{aligned} v_\tau(\alpha, 0) &= 0 \\ u_\tau(0, \beta) &= 0 \\ v_\tau(\alpha, R_\beta \pi/2) &= 0 \end{aligned} \tag{34}$$

and the following boundary conditions are prescribed:

$$v_\tau(a/2, \beta) = w_\tau(a/2, \beta) = 0 \tag{35}$$

with $\tau = 0, 1, ..., N$.

The results are presented for these cases for different thickness ratios $R/h = 2, 4, 10, 100$. A mesh grid of 12×12 elements is taken to ensure the convergence of the solution.

The results lead to similar conclusions made for the plate: the solution converges to the exact solution by increasing the order of expansion N; the LW models are able to give good results, see Tables 6, 7. If one considers the stresses the behavior is the same: higher-order layer wise models are necessary to match the reference solution in the thick shells, see Tables 8, 9. In this case, the use of the LD4 model becomes mandatory. The LD4 model only is able to fulfill the continuity conditions of shear stresses $\sigma_{\alpha z}$ at the interfaces between layers, while lower-order model gives a completely wrong result, even if the shell is very thin ($R/h = 100$), see Figures 21, 22, 25, 26. The LD4 model is not able to fulfill the continuity conditions of transverse stresses σ_{zz} at the interfaces between layers, see Figures 23, 24, 27, 28. To overcome this problem a mixed variational principle could be used. For the description of the electric potential Φ it is necessary to use the higher-order model, LD4, to describe the non-linear behavior of thick shell ($R/h = 2$), see Figures 29, 33, on the other hand for thin shell ($R/h = 100$) a layer-wise description of lower order is sufficient, see Figures 30, 34. The electric displacement $\mathcal{D}_z$ has a non-linear behavior for every thickness ratio in the sensor case, and higher-order models are not sufficient to describe it correctly along the thickness for thick shell ($R/h = 2$), see Figures 31. For the thin cylinder ($R/h = 100$) the continuity interface cannot be reached, see Figure 32. For the actuator case, in spite of its linear behavior, it is necessary an higher-order model to obtain the continuity interface of the electric displacement, see Figures 35, 36. To overcome this problem a mixed variational principle could be used.

7 Conclusion

This paper has presented the static analysis of plate and cylindrical composite structures by means of a shell finite element based on the Unified Formulation by Carrera [39],[40]. The results have been

provided in terms of both displacement, electric potential, transverse stresses and electric displacement, for various thickness ratios from very thick to very thin shells and the performances of the layer-wise theories contained in the CUF have been tested. The conclusions that can be drawn are the following:

1. the shell element is locking free when the shell is very thin;
2. the results converge to the exact solution by increasing the order of expansion of the variables in the thickness;
3. when the shell is very thick, the LW models are able to produce good results;
4. the use of LW models is mandatory for both thick and thin shells, if one needs to accurately describe the distribution of transverse shear and normal stresses and transverse electric displacement in the thickness and to satisfy the interlaminar continuity conditions.
5. the principle of virtual displacement with layer-wise approach is not sufficient to obtain the continuity interface condition for the transverse stresses for thin plate in sensor case and thin shell for sensor and actuator cases, and the transverse electric displacement for thin shell in sensor case.

Future works could be devoted to consider mixed variational principles in the analysis of shell structures with piezo-layers by means of finite elements based on Unified Formulation.

References

[1] Noor AK, Burton WS, *"Assessment of computational models for multilayered shells"*, Appl Mech Rev 1990; 43(4):67-97.

[2] Carrera E, *"Historical review of zig-zag theories for multilayered plates and shells"*, Appl Mech Rev 2003; 56(3):287-308.

[3] Reddy JN, *"Mechanics of laminated composite plates and shells: theory and analysis"*, Boca Raton: CRC Press; 2004.

[4] Carrera E, *"C_z^0 requirements - models for the two dimensional analysis of multilayered structures"*, Compos Struct 1997; 37:373-83.

[5] Koiter WT, *"A consistent first approximation in the general theory of thin elastic shells"*, In: Koiter WT, editor. The theory of thin elastic shells. Delft: IUTAM, North-Holland; 1959, pp. 12-33.

[6] Mindlin RD, *"Forced thickness-shear and flexural vibrations of piezoelectric crystal plates"*, J Appl Phys 1952; 23:83-8.

[7] EerNisse EP, *"Variational method for electroelastic vibration analysis"*, IEEE Trans Sonics Ultrasonics 1967; SU-14(4):153-60.

[8] Tiersten HF, Mindlin RD, *"Forced vibrations of piezoelectric crystal plates"*, Quart Appl Math 1962; 20(2):107-19.

[9] Tiersten HF, *"Linear piezoelectric plate vibrations"*, New York: Plenum; 1969.

[10] Saravanos DA, Heyliger PR, *"Mechanics and computational models for laminated piezoelectric beams, plates and shells"*, Appl Mech Rev 1999; 52(10):305-19.

[11] Kapuria S, *"A coupled zig-zag third-order theory for piezoelectric hybrid cross-ply plates"*, J Appl Mech 2004; 71:604-14.

[12] Ossadzow-David C, Touratier M, *"A multilayered piezoelectric shell theory"*, Compos Sci Technol 2004; 64:2121-37.

[13] Heyliger P, Pei KC, Saravanos DA, *"Layerwise mechanics anLammering:Mesecke-Rischmann:MixedPiezoFEd finite element model for laminated piezoelectric shells"*, AIAA J 1996; 34(11):2353-60.

[14] Ballhause D, D'Ottavio M, Kroplin B, Carrera E, *"A unified formulation to assess multilayered theories for piezoelectric plates"*, Comput Struct 2005; 83(15-16):1217-35.

[15] D'Ottavio M., Ballhause D., Kroeplin B., Carrera E., *"Closed-form solutions for the free-vibration problem of multilayered piezoelectric shells"*, Comput Struct 2006; 84:1506-18.

[16] Benjeddou A, Deu J, Letombe S, *"Free vibrations of simply-supported piezoelectric adaptive plates: An exact sandwich formulation"*, Thin-Walled Struct 2002; 40:573-93.

[17] Rogacheva NN, *"The theory of piezoelectric shells and plates"*, Boca Raton: CRC Press; 1994.

[18] Gopinathan SV, Varadan VV, Varadan VK, *"A review and critique of theories for piezoelectric laminates"*, Smart Mater Struct 2000; 9:24-48.

[19] Benjeddou A, *"Advances in piezoelectric finite element modeling of adaptive structural elements: a survey"*, Comput Struct 2000; 76: 347-63.

[20] Lammering R, Mesecke-Rischmann S, *"Multi-field variational formulations and related finite elements for piezoelectric shells"*, Smart Mater Struct 2003; 12(6):904-13.

[21] Benjeddou A, Andrianarison O, *"Extension of Reissner's mixed variational theorem to piezoelectric multilayered composites"*, In: Lipitakis EA, editor. Proceedings of the sixth Hellenic-European conference on computer mathematics and its applications, LEA, Athens, Hellas, 2003. pp. 116-24.

[22] Sheikh AH, Topdar P., Halder S, *"An appropriate FE model for through-thickness variation of displacement and potential in thin moderately thick smart laminates"*, Comp Struct 2001; 51:401-409.

[23] Auricchio F, Bisegna P, Lovadina C, *"Finite element approximation of piezoelectric plates"*, Int J Numer Meth Engin 2001; 50:1469-1499.

[24] Thornbuegh RP, Chattopadhyay A, *"Simultaneous modeling of mechanical and electrical response of smart composite structures"*, AIAA J 2002; 40(8):1603-1610.

[25] Shu X. *"Free-vibration of laminated piezoelectric composite plates based on an accurate theory"*, Comp Struct 2005; 67:375-382.

[26] Oh J, Cho M, *"A finite element based on cubic zig-zag plate theory for the prediction of thermo-electric-mechanical behaviors"*, Int J Solid Struct 2004; 41(5-6):1357-1375.

[27] Kogl M, Bucalem ML, *"Analysis of smart laminates using piezoelectric MITC plate and shell elements"*, Comput Struct 2005; 83:1153-1163.

[28] Kogl M, Bucalem ML, *"A family of piezoelectric MITC plate elements"*, Comput Struct 2005; 83:1277-1297.

[29] Kulikov GM, Plotnikova SV, *"Exact geometry piezoelectric solid-shell element based on the 7-parameter model"*, Mech Advan Mater Struct 2011; 18:133-146.

[30] Klinkel S, Wagner W, *"A piezoelectric solid shell element based on a mixed variational formulation for geometrically linear and nonlinear applications"*, Comput Struct 2008; 86:38-46.

[31] Carrera E, *"A class of two-dimensional theories for anisotropic multilayered plates analysis,"* Acc Scien di Torino, Memor Scien Fis 1995-1996, pp. 19-20, 1995, pp. 1-39.

[32] Carrera E, *"Theories and finite elements for multilayered plates and shells: a unified compact formulation with numerical assessment and benchmarking"*, Arch Comput Meth Engin 2003; 10(3):215-296.

[33] Garcia Lage R, Mota Soares CM, Mota Soares CA, Reddy JN, *"Modeling of piezoelaminated plates using layerwise mixed finite elements"*, Comput Struct 2004; 82:1849-1863.

[34] D'Ottavio M, Kroplin B, *"An extension of Reissner mixed variational theorem to piezoelectric laminates"*, Mech Advan Mater Struct 2006; 13(2):139-150.

[35] Carrera E, Boscolo M, *"Classical and mixed finite elements for static and dynamics analysis of piezoelectric plates"*, Int J Numer Meth Engin 2007; 70:253-291.

[36] Carrera E, Nali P, *"Mixed piezoelectric plate elements with direct evaluation of transverse electric displacement"*, Int J Numer Meth Engin 2009; 80:403-424.

[37] Bathe KJ, Lee PS, Hiller JF, *"Towards improving the MITC9 shell element"*, Comput Struct 2003; 81:477-489.

[38] Panasz P Wisniewski K, *"Nine-node shell elements with 6 dofs/node based on two-level approximations. Part I Theory and linear tests"*, Fin Elem Anal Des 2008; 44:784-796.

[39] Carrera E, *"Multilayered shell theories accounting for layerwise mixed description, Part 1: governing equations"*, AIAA J 1999; 37(9):1107-1116.

[40] Carrera E, *"Multilayered shell theories accounting for layerwise mixed description, Part 2: numerical evaluations"*, AIAA J 1999; 37(9):1117-1124.

[41] Bathe K-J, Dvorkin E, *"A formulation of general shell elements - the use of mixed interpolation of tensorial components"*, Int J Numer Meth Engin 1986; 22:697-722.

[42] Bucalem ML, Bathe, K-J, *"Higher-order MITC general shell elements"*, Int J Numer Meth Engin 1993; 36:3729-3754.

[43] Carrera E, Brischetto S, *"Piezoelectric shell theories with a priori continous transverse electromechanical variables"*, J Mech Mater Struct 2007; 2(2):377-399.

Explicit form of stiffness fundamental nucleus

In order to write the fundamental nucleus $\boldsymbol{K}^{k\tau sij}$ in compact form, the following integrals in the domain Ω_k are defined:

$$\left(W^k_{m1\,n1}\,;\,W^k_{m1\,n2}\,;\,W^k_{m2\,n1}\,;\,W^k_{m2\,n2}\right)=\int\limits_{\Omega_k}\left(N_{m1}N_{n1}\,;\,N_{m1}N_{n2}\,;\,N_{m2}N_{n1}\,;\,N_{m2}N_{n2}\right)d\alpha\,d\beta$$

$$\left(W^k_{m1\,n3}\,;\,W^k_{m3\,n1}\,;\,W^k_{m3\,n3}\,;\,W^k_{m2\,n3}\,;\,W^k_{m3\,n2}\right)=\int\limits_{\Omega_k}\left(N_{m1}N_{n3}\,;\,N_{m3}N_{n1}\,;\,N_{m3}N_{n3}\,;\,N_{m2}N_{n3}\,;\,N_{m3}N_{n2}\right)d\alpha\,d\beta$$

$$\left(W^k_{m1\,j}\,;\,W^k_{m2\,j}\,;\,W^k_{m3\,j}\right)=\int\limits_{\Omega_k}\left(N_{m1}N_{j}\,;\,N_{m2}N_{j}\,;\,N_{m3}N_{j}\right)d\alpha\,d\beta$$

$$\left(W^k_{i\,n1}\,;\,W^k_{i\,n2}\,;\,W^k_{i\,n3}\,;\,W^k_{i\,j}\right)=\int\limits_{\Omega_k}\left(N_{i}N_{n1}\,;\,N_{i}N_{n2}\,;\,N_{i}N_{n3}\,;\,N_{i}N_{j}\right)d\alpha\,d\beta$$

$$\left(W^k_{m1\,j,_\alpha}\,;\,W^k_{m1\,j,_\beta}\,;\,W^k_{m2\,j,_\alpha}\,;\,W^k_{m2\,j,_\beta}\right)=\int\limits_{\Omega_k}\left(N_{m1}\frac{\partial N_j}{\partial\alpha}\,;\,N_{m1}\frac{\partial N_j}{\partial\beta}\,;\,N_{m2}\frac{\partial N_j}{\partial\alpha}\,;\,N_{m2}\frac{\partial N_j}{\partial\beta}\right)d\alpha\,d\beta$$

$$\left(W^k_{i,_\alpha\,n1}\,;\,W^k_{i,_\beta\,n1}\,;\,W^k_{i,_\alpha\,n2}\,;\,W^k_{i,_\beta\,n2}\right)=\int\limits_{\Omega_k}\left(\frac{\partial N_i}{\partial\alpha}N_{n1}\,;\,\frac{\partial N_i}{\partial\beta}N_{n1}\,;\,\frac{\partial N_i}{\partial\alpha}N_{n2}\,;\,\frac{\partial N_i}{\partial\beta}N_{n2}\right)d\alpha\,d\beta$$

Moreover, the integrals on the domain A_k, in the thickness direction, are written as:

$$\left(J^{k\tau s},J^{k\tau s}_\alpha,J^{k\tau s}_\beta,J^{k\tau s}_{\frac{\alpha}{\beta}},J^{k\tau s}_{\frac{\beta}{\alpha}},J^{k\tau s}_{\alpha\beta}\right)=\int\limits_{A_k}F_\tau F_s\left(1,H^k_\alpha,H^k_\beta,\frac{H^k_\alpha}{H^k_\beta},\frac{H^k_\beta}{H^k_\alpha},H^k_\alpha H^k_\beta\right)dz$$

$$\left(J^{k\tau_z s},J^{k\tau_z s}_\alpha,J^{k\tau_z s}_\beta,J^{k\tau_z s}_{\frac{\alpha}{\beta}},J^{k\tau_z s}_{\frac{\beta}{\alpha}},J^{k\tau_z s}_{\alpha\beta}\right)=\int\limits_{A_k}\frac{\partial F_\tau}{\partial z}F_s\left(1,H^k_\alpha,H^k_\beta,\frac{H^k_\alpha}{H^k_\beta},\frac{H^k_\beta}{H^k_\alpha},H^k_\alpha H^k_\beta\right)dz$$

$$\left(J^{k\tau s_z},J^{k\tau s_z}_\alpha,J^{k\tau s_z}_\beta,J^{k\tau s_z}_{\frac{\alpha}{\beta}},J^{k\tau s_z}_{\frac{\beta}{\alpha}},J^{k\tau s_z}_{\alpha\beta}\right)=\int\limits_{A_k}F_\tau\frac{\partial F_s}{\partial z}\left(1,H^k_\alpha,H^k_\beta,\frac{H^k_\alpha}{H^k_\beta},\frac{H^k_\beta}{H^k_\alpha},H^k_\alpha H^k_\beta\right)dz$$

$$\left(J^{k\tau_z s_z}, J^{k\tau_z s_z}_{\alpha}, J^{k\tau_z s_z}_{\beta}, J^{k\tau_z s_z}_{\frac{\alpha}{\beta}}, J^{k\tau_z s_z}_{\frac{\beta}{\alpha}}, J^{k\tau_z s_z}_{\alpha\beta}\right) = \int\limits_{A_k} \frac{\partial F_\tau}{\partial z}\frac{\partial F_s}{\partial z}\left(1, H^k_\alpha, H^k_\beta, \frac{H^k_\alpha}{H^k_\beta}, \frac{H^k_\beta}{H^k_\alpha}, H^k_\alpha H^k_\beta\right) dz$$

The stiffness fundamental nucleus $\boldsymbol{K}^{\tau sij}$ is:

$$\boldsymbol{K}^{k\tau sij} = \begin{bmatrix} \boldsymbol{K}_{11} & \boldsymbol{K}_{12} & \boldsymbol{K}_{13} & \boldsymbol{K}_{14} \\ \boldsymbol{K}_{21} & \boldsymbol{K}_{22} & \boldsymbol{K}_{23} & \boldsymbol{K}_{24} \\ \boldsymbol{K}_{31} & \boldsymbol{K}_{32} & \boldsymbol{K}_{33} & \boldsymbol{K}_{34} \\ \boldsymbol{K}_{41} & \boldsymbol{K}_{42} & \boldsymbol{K}_{43} & \boldsymbol{K}_{44} \end{bmatrix}^{k\tau sij}$$

The elements of the nucleus are:

$$\begin{aligned} K^{k\tau s}_{uu_{11}} = {} & C^k_{55}\, N^{(m1)}_i N^{(n1)}_j\, W^k_{m1\,n1}\, J^{k\tau_z s_z}_{\alpha\beta} - \frac{C^k_{55}}{R^k_\alpha}\, N^{(m1)}_i N^{(n1)}_j\, W^k_{m1\,n1}\, J^{k\tau_z s}_{\beta} - \frac{C^k_{55}}{R^k_\alpha}\, N^{(m1)}_i N^{(n1)}_j\, W^k_{m1\,n1}\, J^{k\tau s_z}_{\beta} + \\ & + C^k_{66}\, N^{(m3)}_{i,\beta} N^{(n3)}_{j,\beta}\, W^k_{m3\,n3}\, J^{k\tau s}_{\frac{\alpha}{\beta}} + C^k_{16}\, N^{(m1)}_{i,\alpha} N^{(n3)}_{j,\beta}\, W^k_{m1\,n3}\, J^{k\tau s} + C^k_{16}\, N^{(m3)}_{i,\beta} N^{(n1)}_{j,\alpha}\, W^k_{m3\,n1}\, J^{k\tau s} + \\ & + C^k_{11}\, N^{(m1)}_{i,\alpha} N^{(n1)}_{j,\alpha}\, W^k_{m1\,n1}\, J^{k\tau s}_{\frac{\beta}{\alpha}} + \frac{C^k_{55}}{(R^k_\alpha)^2}\, N^{(m1)}_i N^{(n1)}_j\, W^k_{m1\,n1}\, J^{k\tau s}_{\frac{\beta}{\alpha}} \end{aligned}$$

$$\begin{aligned} K^{k\tau s}_{uu_{12}} = {} & C^k_{45}\, N^{(m1)}_i N^{(n2)}_j\, W^k_{m1\,n2}\, J^{k\tau_z s_z}_{\alpha\beta} - \frac{C^k_{45}}{R^k_\beta}\, N^{(m1)}_i N^{(n2)}_j\, W^k_{m1\,n2}\, J^{k\tau_z s}_{\alpha} - \frac{C^k_{45}}{R^k_\alpha}\, N^{(m1)}_i N^{(n2)}_j\, W^k_{m1\,n2}\, J^{k\tau s_z}_{\beta} + \\ & + C^k_{26}\, N^{(m3)}_{i,\beta} N^{(n2)}_{j,\beta}\, W^k_{m3\,n2}\, J^{k\tau s}_{\frac{\alpha}{\beta}} + C^k_{12}\, N^{(m1)}_{i,\alpha} N^{(n2)}_{j,\beta}\, W^k_{m1\,n2}\, J^{k\tau s} + C^k_{66}\, N^{(m3)}_{i,\beta} N^{(n3)}_{j,\alpha}\, W^k_{m3\,n3}\, J^{k\tau s} + \\ & + C^k_{16}\, N^{(m1)}_{i,\alpha} N^{(n3)}_{j,\alpha}\, W^k_{m1\,n3}\, J^{k\tau s}_{\frac{\beta}{\alpha}} + \frac{C^k_{45}}{R^k_\alpha R^k_\beta}\, N^{(m1)}_i N^{(n2)}_j\, W^k_{m1\,n2}\, J^{k\tau s} \end{aligned}$$

$$\begin{aligned} K^{k\tau s}_{uu_{13}} = {} & C^k_{45}\, N^{(m1)}_i N^{(n2)}_{j,\beta}\, W^k_{m1\,n2}\, J^{k\tau_z s}_{\alpha} + C^k_{55}\, N^{(m1)}_i N^{(n1)}_{j,\alpha}\, W^k_{m1\,n1}\, J^{k\tau_z s}_{\beta} + C^k_{36}\, N^{(m3)}_{i,\beta}\, W^k_{m3\,j}\, J^{k\tau s_z}_{\alpha} + \\ & + C^k_{13}\, N^{(m1)}_{i,\alpha}\, W^k_{m1\,j}\, J^{k\tau s_z}_{\beta} - \frac{C^k_{45}}{R^k_\alpha}\, N^{(m1)}_i N^{(n2)}_{j,\beta}\, W^k_{m1\,n2}\, J^{k\tau s} - \frac{C^k_{55}}{R^k_\alpha}\, N^{(m1)}_i N^{(n1)}_{j,\alpha}\, W^k_{m1\,n1}\, J^{k\tau s}_{\frac{\beta}{\alpha}} + \\ & + \frac{C^k_{26}}{R^k_\beta}\, N^{(m3)}_{i,\beta} N^{(n2)}_j\, W^k_{m3\,n2}\, J^{k\tau s}_{\frac{\alpha}{\beta}} + \frac{C^k_{16}}{R^k_\alpha}\, N^{(m3)}_{i,\beta} N^{(n1)}_j\, W^k_{m3\,n1}\, J^{k\tau s} + \frac{C^k_{12}}{R^k_\beta}\, N^{(m1)}_{i,\alpha} N^{(n2)}_j\, W^k_{m1\,n2}\, J^{k\tau s} + \\ & + \frac{C^k_{11}}{R^k_\alpha}\, N^{(m1)}_{i,\alpha} N^{(n1)}_j\, W^k_{m1\,n1}\, J^{k\tau s}_{\frac{\beta}{\alpha}} \end{aligned} \tag{A.36}$$

$$K^{k\tau s}_{uu_{21}} = C^k_{45}\, N^{(m2)}_i N^{(n1)}_j\, W^k_{m2\,n1}\, J^{k\tau_z s_z}_{\alpha\beta} - \frac{C^k_{45}}{R^k_\alpha}\, N^{(m2)}_i N^{(n1)}_j\, W^k_{m2\,n1}\, J^{k\tau_z s}_{\beta} - \frac{C^k_{45}}{R^k_\beta}\, N^{(m2)}_i N^{(n1)}_j\, W^k_{m2\,n1}\, J^{k\tau s_z}_{\alpha} +$$
$$+ C^k_{26}\, N^{(m2)}_{i,\beta} N^{(n3)}_{j,\beta}\, W^k_{m2\,n3}\, J^{k\tau s}_{\frac{\alpha}{\beta}} + C^k_{66}\, N^{(m3)}_{i,\alpha} N^{(n3)}_{j,\beta}\, W^k_{m3\,n3}\, J^{k\tau s} + C^k_{12}\, N^{(m2)}_{i,\beta} N^{(n1)}_{j,\alpha}\, W^k_{m2\,n1}\, J^{k\tau s} +$$
$$+ C^k_{16}\, N^{(m3)}_{i,\alpha} N^{(n1)}_{j,\alpha}\, W^k_{m3\,n1}\, J^{k\tau s}_{\frac{\beta}{\alpha}} + \frac{C^k_{45}}{R^k_\alpha R^k_\beta}\, N^{(m2)}_i N^{(n1)}_j\, W^k_{m2\,n1}\, J^{k\tau s}$$

$$K^{k\tau s}_{uu_{22}} = C^k_{44}\, N^{(m2)}_i N^{(n2)}_j\, W^k_{m2\,n2}\, J^{k\tau_z s_z}_{\alpha\beta} - \frac{C^k_{44}}{R^k_\beta}\, N^{(m2)}_i N^{(n2)}_j\, W^k_{m2\,n2}\, J^{k\tau_z s}_{\alpha} - \frac{C^k_{44}}{R^k_\beta}\, N^{(m2)}_i N^{(n2)}_j\, W^k_{m2\,n2}\, J^{k\tau s_z}_{\alpha} +$$
$$+ C^k_{22}\, N^{(m2)}_{i,\beta} N^{(n2)}_{j,\beta}\, W^k_{m2\,n2}\, J^{k\tau s}_{\frac{\alpha}{\beta}} + C^k_{26}\, N^{(m3)}_{i,\alpha} N^{(n2)}_{j,\beta}\, W^k_{m3\,n2}\, J^{k\tau s} + C^k_{26}\, N^{(m2)}_{i,\beta} N^{(n3)}_{j,\alpha}\, W^k_{m2\,n3}\, J^{k\tau s} +$$
$$+ C^k_{66}\, N^{(m3)}_{i,\alpha} N^{(n3)}_{j,\alpha}\, W^k_{m3\,n3}\, J^{k\tau s}_{\frac{\beta}{\alpha}} + \frac{C^k_{44}}{\left(R^k_\beta\right)^2}\, N^{(m2)}_i N^{(n2)}_j\, W^k_{m2\,n2}\, J^{k\tau s}_{\frac{\alpha}{\beta}}$$

$$K^{k\tau s}_{uu_{23}} = C^k_{44}\, N^{(m2)}_i N^{(n2)}_{j,\beta}\, W^k_{m2\,n2}\, J^{k\tau_z s}_{\alpha} + C^k_{45}\, N^{(m2)}_i N^{(n1)}_{j,\alpha}\, W^k_{m2\,n1}\, J^{k\tau_z s}_{\beta} + C^k_{23}\, N^{(m2)}_{i,\beta}\, W^k_{m2\,j}\, J^{k\tau s_z}_{\alpha} +$$
$$+ C^k_{36}\, N^{(m3)}_{i,\alpha}\, W^k_{m3\,j}\, J^{k\tau s_z}_{\beta} - \frac{C^k_{44}}{R^k_\beta}\, N^{(m2)}_i N^{(n2)}_{j,\beta}\, W^k_{m2\,n2}\, J^{k\tau s}_{\frac{\alpha}{\beta}} - \frac{C^k_{45}}{R^k_\beta}\, N^{(m2)}_i N^{(n1)}_{j,\alpha}\, W^k_{m2\,n1}\, J^{k\tau s} +$$
$$+ \frac{C^k_{22}}{R^k_\beta}\, N^{(m2)}_{i,\beta} N^{(n2)}_j\, W^k_{m2\,n2}\, J^{k\tau s}_{\frac{\alpha}{\beta}} + \frac{C^k_{12}}{R^k_\alpha}\, N^{(m2)}_{i,\beta} N^{(n1)}_j\, W^k_{m2\,n1}\, J^{k\tau s} + \frac{C^k_{26}}{R^k_\beta}\, N^{(m3)}_{i,\alpha} N^{(n2)}_j\, W^k_{m3\,n2}\, J^{k\tau s} +$$
$$+ \frac{C^k_{16}}{R^k_\alpha}\, N^{(m3)}_{i,\alpha} N^{(n1)}_j\, W^k_{m3\,n1}\, J^{k\tau s}_{\frac{\beta}{\alpha}}$$

$$K^{k\tau s}_{uu_{31}} = C^k_{36}\, N^{(n3)}_{j,\beta}\, W^k_{i\,n3}\, J^{k\tau_z s}_{\alpha} + C^k_{13}\, N^{(n1)}_{j,\alpha}\, W^k_{i\,n1}\, J^{k\tau_z s}_{\beta} + C^k_{45}\, N^{(m2)}_{i,\beta} N^{(n1)}_j\, W^k_{m2\,n1}\, J^{k\tau s_z}_{\alpha} +$$
$$+ C^k_{55}\, N^{(m1)}_{i,\alpha} N^{(n1)}_j\, W^k_{m1\,n1}\, J^{k\tau s_z}_{\beta} + \frac{C^k_{26}}{R^k_\beta}\, N^{(m2)}_i N^{(n3)}_{j,\beta}\, W^k_{m2\,n3}\, J^{k\tau s}_{\frac{\alpha}{\beta}} + \frac{C^k_{16}}{R^k_\alpha}\, N^{(m1)}_i N^{(n3)}_{j,\beta}\, W^k_{m1\,n3}\, J^{k\tau s} +$$
$$+ \frac{C^k_{12}}{R^k_\beta}\, N^{(m2)}_i N^{(n1)}_{j,\alpha}\, W^k_{m2\,n1}\, J^{k\tau s} + \frac{C^k_{11}}{R^k_\alpha}\, N^{(m1)}_i N^{(n1)}_{j,\alpha}\, W^k_{m1\,n1}\, J^{k\tau s}_{\frac{\beta}{\alpha}} - \frac{C^k_{45}}{R^k_\alpha}\, N^{(m2)}_{i,\beta} N^{(n1)}_j\, W^k_{m2\,n1}\, J^{k\tau s} -$$
$$- \frac{C^k_{55}}{R^k_\alpha}\, N^{(m1)}_{i,\alpha} N^{(n1)}_j\, W^k_{m1\,n1}\, J^{k\tau s}_{\frac{\beta}{\alpha}}$$

$$K^{k\tau s}_{uu_{32}} = C^k_{23}\, N^{(n2)}_{j,\beta}\, W^k_{i\,n2}\, J^{k\tau_z s}_{\alpha} + C^k_{36}\, N^{(n3)}_{j,\alpha}\, W^k_{i\,n3}\, J^{k\tau_z s}_{\beta} + C^k_{44}\, N^{(m2)}_{i,\beta} N^{(n2)}_{j}\, W^k_{m2\,n2}\, J^{k\tau s_z}_{\alpha} +$$
$$+ C^k_{45}\, N^{(m1)}_{i,\alpha} N^{(n2)}_{j}\, W^k_{m1\,n2}\, J^{k\tau s_z}_{\beta} + \frac{C^k_{22}}{R^k_{\beta}}\, N^{(m2)}_{i} N^{(n2)}_{j,\beta}\, W^k_{m2\,n2}\, J^{k\tau s}_{\frac{\alpha}{\beta}} + \frac{C^k_{12}}{R^k_{\alpha}}\, N^{(m1)}_{i} N^{(n2)}_{j,\beta}\, W^k_{m1\,n2}\, J^{k\tau s} +$$
$$+ \frac{C^k_{26}}{R^k_{\beta}}\, N^{(m2)}_{i} N^{(n3)}_{j,\alpha}\, W^k_{m2\,n3}\, J^{k\tau s} + \frac{C^k_{16}}{R^k_{\alpha}}\, N^{(m1)}_{i} N^{(n3)}_{j,\alpha}\, W^k_{m1\,n3}\, J^{k\tau s}_{\frac{\beta}{\alpha}} - \frac{C^k_{44}}{R^k_{\beta}}\, N^{(m2)}_{i,\beta} N^{(n2)}_{j}\, W^k_{m2\,n2}\, J^{k\tau s}_{\frac{\alpha}{\beta}} -$$
$$- \frac{C^k_{45}}{R^k_{\beta}}\, N^{(m1)}_{i,\alpha} N^{(n2)}_{j}\, W^k_{m1\,n2}\, J^{k\tau s}$$

$$K^{k\tau s}_{uu_{33}} = C^k_{33}\, W^k_{i\,j}\, J^{k\tau_z s_z}_{\alpha\beta} + \frac{C^k_{23}}{R^k_{\beta}}\, N^{(n2)}_{j}\, W^k_{i\,n2}\, J^{k\tau_z s}_{\alpha} + \frac{C^k_{13}}{R^k_{\alpha}}\, N^{(n1)}_{j}\, W^k_{i\,n1}\, J^{k\tau_z s}_{\beta} +$$
$$+ \frac{C^k_{23}}{R^k_{\beta}}\, N^{(m2)}_{i}\, W^k_{m2\,j}\, J^{k\tau s_z}_{\alpha} + \frac{C^k_{13}}{R^k_{\alpha}}\, N^{(m1)}_{i}\, W^k_{m1\,j}\, J^{k\tau s_z}_{\beta} + C^k_{44}\, N^{(m2)}_{i,\beta} N^{(n2)}_{j,\beta}\, W^k_{m2\,n2}\, J^{k\tau s}_{\frac{\alpha}{\beta}} +$$
$$+ C^k_{45}\, N^{(m1)}_{i,\alpha} N^{(n2)}_{j,\beta}\, W^k_{m1\,n2}\, J^{k\tau s} + C^k_{45}\, N^{(m2)}_{i,\beta} N^{(n1)}_{j,\alpha}\, W^k_{m2\,n1}\, J^{k\tau s} + C^k_{55}\, N^{(m1)}_{i,\alpha} N^{(n1)}_{j,\alpha}\, W^k_{m1\,n1}\, J^{k\tau s}_{\frac{\beta}{\alpha}} +$$
$$+ \frac{C^k_{12}}{R^k_{\alpha} R^k_{\beta}}\, N^{(m1)}_{i} N^{(n2)}_{j}\, W^k_{m1\,n2}\, J^{k\tau s} + \frac{C^k_{12}}{R^k_{\alpha} R^k_{\beta}}\, N^{(m2)}_{i} N^{(n1)}_{j}\, W^k_{m2\,n1}\, J^{k\tau s} +$$
$$+ \frac{C^k_{22}}{\left(R^k_{\beta}\right)^2}\, N^{(m2)}_{i} N^{(n2)}_{j}\, W^k_{m2\,n2}\, J^{k\tau s}_{\frac{\alpha}{\beta}} + \frac{C^k_{11}}{\left(R^k_{\alpha}\right)^2}\, N^{(m1)}_{i} N^{(n1)}_{j}\, W^k_{m1\,n1}\, J^{k\tau s}_{\frac{\beta}{\alpha}}$$

$$K^{k\tau s}_{u\Phi_{14}} = e^k_{25}\, N^{(m1)}_{i}\, W^k_{m1\,j,\beta}\, J^{k\tau_z s}_{\alpha} + e^k_{15}\, N^{(m1)}_{i}\, W^k_{m1\,j,\alpha}\, J^{k\tau_z s}_{\beta} + e^k_{36}\, N^{(m3)}_{i,\beta}\, W^k_{m3\,j}\, J^{k\tau s_z}_{\alpha} +$$
$$+ e^k_{31}\, N^{(m1)}_{i,\alpha}\, W^k_{m1\,j}\, J^{k\tau s_z}_{\beta} - \frac{e^k_{25}}{R^k_{\alpha}}\, N^{(m1)}_{i}\, W^k_{m1\,j,\beta}\, J^{k\tau s} - \frac{e^k_{15}}{R^k_{\alpha}}\, N^{(m1)}_{i}\, W^k_{m1\,j,\alpha}\, J^{k\tau s}_{\frac{\beta}{\alpha}}$$

$$K^{k\tau s}_{u\Phi_{24}} = e^k_{24}\, N^{(m2)}_{i}\, W^k_{m2\,j,\beta}\, J^{k\tau_z s}_{\alpha} + e^k_{14}\, N^{(m2)}_{i}\, W^k_{m2\,j,\alpha}\, J^{k\tau_z s}_{\beta} + e^k_{32}\, N^{(m2)}_{i,\beta}\, W^k_{m2\,j}\, J^{k\tau s_z}_{\alpha} +$$
$$+ e^k_{36}\, N^{(m3)}_{i,\alpha}\, W^k_{m3\,j}\, J^{k\tau s_z}_{\beta} - \frac{e^k_{24}}{R^k_{\beta}}\, N^{(m2)}_{i}\, W^k_{m2\,j,\beta}\, J^{k\tau s}_{\frac{\alpha}{\beta}} - \frac{e^k_{14}}{R^k_{\beta}}\, N^{(m2)}_{i}\, W^k_{m2\,j,\alpha}\, J^{k\tau s}$$

$$K^{k\tau s}_{u\Phi_{34}} = e^k_{33}\, W^k_{i\,j}\, J^{k\tau_z s_z}_{\alpha\beta} + \frac{e^k_{32}}{R^k_{\beta}}\, N^{(m2)}_{i}\, W^k_{m2\,j}\, J^{k\tau s_z}_{\alpha} + \frac{e^k_{31}}{R^k_{\alpha}}\, N^{(m1)}_{i}\, W^k_{m1\,j}\, J^{k\tau s_z}_{\beta} +$$
$$+ e^k_{24}\, N^{(m2)}_{i,\beta}\, W^k_{m2\,j,\beta}\, J^{k\tau s}_{\frac{\alpha}{\beta}} + e^k_{25}\, N^{(m1)}_{i,\alpha}\, W^k_{m1\,j,\beta}\, J^{k\tau s} + e^k_{14}\, N^{(m2)}_{i,\beta}\, W^k_{m2\,j,\alpha}\, J^{k\tau s} +$$
$$+ e^k_{15}\, N^{(m1)}_{i,\alpha}\, W^k_{m1\,j,\alpha}\, J^{k\tau s}_{\frac{\beta}{\alpha}}$$

$$K^{k\tau s}_{\Phi u_{41}} = e^k_{36}\, N^{(n3)}_{j,\beta}\, W^k_{i\, n3}\, J^{k\tau_z s}_{\alpha} + e^k_{31}\, N^{(n1)}_{j,\alpha}\, W^k_{i\, n1}\, J^{k\tau_z s}_{\beta} + e^k_{25}\, N^{(n1)}_{j}\, W^k_{i,\beta\, n1}\, J^{k\tau s_z}_{\alpha} +$$
$$+ e^k_{15}\, N^{(n1)}_{j}\, W^k_{i,\alpha\, n1}\, J^{k\tau s_z}_{\beta} - \frac{e^k_{25}}{R^k_{\alpha}}\, N^{(n1)}_{j}\, W^k_{i,\beta\, n1}\, J^{k\tau s} - \frac{e^k_{15}}{R^k_{\alpha}}\, N^{(n1)}_{j}\, W^k_{i,\alpha\, n1}\, J^{k\tau s}_{\frac{\beta}{\alpha}}$$

$$K^{k\tau s}_{\Phi u_{42}} = e^k_{32}\, N^{(n2)}_{j,\beta}\, W^k_{i\, n2}\, J^{k\tau_z s}_{\alpha} + e^k_{36}\, N^{(n3)}_{j,\alpha}\, W^k_{i\, n3}\, J^{k\tau_z s}_{\beta} + e^k_{24}\, N^{(n2)}_{j}\, W^k_{i,\beta\, n2}\, J^{k\tau s_z}_{\alpha} +$$
$$+ e^k_{14}\, N^{(n2)}_{j}\, W^k_{i,\alpha\, n2}\, J^{k\tau s_z}_{\beta} - \frac{e^k_{24}}{R^k_{\beta}}\, N^{(n2)}_{j}\, W^k_{i,\beta\, n2}\, J^{k\tau s}_{\frac{\alpha}{\beta}} - \frac{e^k_{14}}{R^k_{\beta}}\, N^{(n2)}_{j}\, W^k_{i,\alpha\, n2}\, J^{k\tau s}$$

$$K^{k\tau s}_{\Phi u_{43}} = e^k_{33}\, W^k_{i\, j}\, J^{k\tau_z s_z}_{\alpha\beta} + \frac{e^k_{32}}{R^k_{\beta}}\, N^{(n2)}_{j}\, W^k_{i\, n2}\, J^{k\tau_z s}_{\alpha} + \frac{e^k_{31}}{R^k_{\alpha}}\, N^{(n1)}_{j}\, W^k_{i\, n1}\, J^{k\tau_z s}_{\beta} +$$
$$+ e^k_{24}\, N^{(n2)}_{j,\beta}\, W^k_{i,\beta\, n2}\, J^{k\tau s}_{\frac{\alpha}{\beta}} + e^k_{14}\, N^{(n2)}_{j,\beta}\, W^k_{i,\alpha\, n2}\, J^{k\tau s} + e^k_{25}\, N^{(n1)}_{j,\alpha}\, W^k_{i,\beta\, n1}\, J^{k\tau s} +$$
$$+ e^k_{15}\, N^{(n1)}_{j,\alpha}\, W^k_{i,\alpha\, n1}\, J^{k\tau s}_{\frac{\beta}{\alpha}}$$

$$K^{k\tau s}_{\Phi\Phi_{44}} = -\varepsilon^k_{33}\, W^k_{i\, j}\, J^{k\tau_z s_z}_{\alpha\beta} - \varepsilon^k_{22}\, W^k_{i,\beta\, j,\beta}\, J^{k\tau s}_{\frac{\alpha}{\beta}} - \varepsilon^k_{12}\, W^k_{i,\alpha\, j,\beta}\, J^{k\tau s} - \varepsilon^k_{12}\, W^k_{i,\beta\, j,\alpha}\, J^{k\tau s} -$$
$$- \varepsilon^k_{11}\, W^k_{i,\alpha\, j,\alpha}\, J^{k\tau s}_{\frac{\beta}{\alpha}}$$

Properties	PZT-4	Gr/EP
$E_{11}\,[GPa]$	81.3	132.38
$E_{22}\,[GPa]$	81.3	10.756
$E_{33}\,[GPa]$	64.5	10.756
$\nu_{12}\,[-]$	0.329	0.24
$\nu_{13}\,[-]$	0.432	0.24
$\nu_{23}\,[-]$	0.432	0.49
$G_{44}\,[GPa]$	25.6	3.606
$G_{55}\,[GPa]$	25.6	5.6537
$G_{66}\,[GPa]$	30.6	5.6537
$e_{15}\,[C/m^2]$	12.72	0
$e_{24}\,[C/m^2]$	12.72	0
$e_{31}\,[C/m^2]$	-5.20	0
$e_{32}\,[C/m^2]$	-5.20	0
$e_{33}\,[C/m^2]$	15.08	0
$\tilde{\epsilon}_{11}/\epsilon_0\,[-]$	1475	3.5
$\tilde{\epsilon}_{22}/\epsilon_0\,[-]$	1475	3.0
$\tilde{\epsilon}_{33}/\epsilon_0\,[-]$	1300	3.0

Table 1: Physical data for multilayered plate and cylindrical shell.

		$a\,/\,h$	2	4	10	100
$\boldsymbol{Ref.}$[14]	$\boldsymbol{w}$	$LD4_a$	4.9113	30.029	582.06	4675300
		$FSDT_a$	2.8575	18.488	423.29	3668700
	$\boldsymbol{\Phi}$	$LD4_a$	0.9103	6.1084	44.471	4580.2
		$FSDT_a$	0.78657	2.6580	15.044	1470.3
	$\boldsymbol{\mathcal{D}_z}$	$LD4_a$	0.0256	0.0161	0.0139	0.0136
		$FSDT_a$	0.0615	0.0401	-0.1174	-18.729
	$\boldsymbol{w}$	LD4	4.9112	30.0286	582.1298	4675118.5
		LD3	4.9112	30.0285	582.1298	4675118.5
		LD2	4.8954	29.9812	581.8951	4675095.5
		LD1	4.8087	29.8512	579.2426	4647075.5
	$\boldsymbol{\Phi}$	LD4	0.9106	6.1107	44.4934	4586.8311
		LD3	0.9103	6.1102	44.4920	4586.8311
		LD2	0.8948	6.0899	44.4760	4586.7891
		LD1	0.8599	6.0320	44.1802	4559.1191
	$\boldsymbol{\mathcal{D}_z}$	LD4	0.0252	0.0140	0.0051	-0.0140
		LD3	0.0255	0.0142	0.0054	-0.0144
		LD2	0.0271	0.0156	0.0064	-0.0205
		LD1	-0.0665	-0.0890	-0.2905	-23.8867

Table 2: Transverse normal displacement $\boldsymbol{w} * 10^{11}$ evaluated along the thickness in $(z = 0)$. Electric potential $\boldsymbol{\Phi} * 10^3$ evaluated along the thickness in $(z = 0)$. Transverse normal electric displacement $\boldsymbol{\mathcal{D}_z} * 10^9$ evaluated along the thickness at *top* $(z = +h/2)$. Plate with 4 layers. Sensor case.

		$a\,/\,h$	2	4	10	100
Ref.[14]	$\boldsymbol{\sigma_{xx}}$	$LD4_a$	3.2207	6.5642	32.771	3142.1
	$\boldsymbol{\sigma_{xz}}$	$LD4_a$	-0.26995	-0.68720	-1.8540	-18.832
	$\boldsymbol{\sigma_{xx}}$	LD4	3.2240	6.5710	32.8145	3146.8381
		LD3	3.2263	6.5719	32.8153	3146.8376
		LD2	3.2088	6.5659	32.8137	3146.8433
		LD1	3.5228	7.0093	34.3028	3271.7583
	$\boldsymbol{\sigma_{xz}}$	LD4	-0.2758	-0.6902	-1.8576	-18.8640
		LD3	-0.2697	-0.6862	-1.8560	-18.8638
		LD2	-0.3620	-0.8157	-2.1371	-21.6073
		LD1	-0.3165	-0.7094	-1.8693	-18.9304
	$\boldsymbol{\sigma_{zz}}$	LD4	1.0001	1.0001	1.0001	0.9955
		LD3	1.0052	1.0015	1.0008	0.9957
		LD2	1.0334	1.0268	1.0270	1.0757
		LD1	2.1237	2.3562	5.1631	342.3075

Table 3: Principal stresses $\boldsymbol{\sigma_{xx}}$, $\boldsymbol{\sigma_{zz}}$ evaluated along the thickness at *top* ($z = +h/2$) and shear stress $\boldsymbol{\sigma_{xz}}$ evaluated along the thickness in ($z = 0$). Plate with 4 layers. Sensor case.

		$a\,/\,h$	2	4	10	100
Ref.[14]	$\boldsymbol{w}$	$LD4_a$	-1.7475	-1.4707	-1.3697	-1.3493
		$FSDT_a$	-13.923	-14.107	-14.159	-14.169
	$\boldsymbol{\Phi}$	$LD4_a$	0.3330	0.4477	0.4910	0.4999
		$FSDT_a$	0.3219	0.4461	0.4908	0.4999
	$\boldsymbol{\mathcal{D}_z}$	$LD4_a$	-9.4085	-2.4184	-0.4168	-0.0370
		$FSDT_a$	-3.6667	-0.9566	-0.1816	-0.0347
	$\boldsymbol{w}$	LD4	-1.7476	-1.4708	-1.3697	-1.3494
		LD3	-1.7476	-1.4707	-1.3697	-1.3494
		LD2	-1.7291	-1.4663	-1.3691	-1.3493
		LD1	-2.1030	-1.5963	-1.4297	-1.3971
	$\boldsymbol{\Phi}$	LD4	0.3330	0.4477	0.4910	0.4999
		LD3	0.3330	0.4477	0.4910	0.4999
		LD2	0.3331	0.4477	0.4910	0.4999
		LD1	0.3241	0.4468	0.4910	0.4999
	$\boldsymbol{\mathcal{D}_z}$	LD4	-9.4104	-2.4185	-0.4167	-0.0370
		LD3	-9.4047	-2.4182	-0.4167	-0.0370
		LD2	-9.3822	-2.4167	-0.4166	-0.0370
		LD1	-5.2969	-1.3815	-0.2504	-0.0353

Table 4: Transverse normal displacement $\boldsymbol{w} * 10^{11}$ evaluated along the thickness in $(z = 0)$. Electric potential $\boldsymbol{\Phi}$ evaluated along the thickness in $(z = 0)$. Transverse normal electric displacement $\boldsymbol{\mathcal{D}_z} * 10^9$ evaluated along the thickness at *top* $(z = +h/2)$. Plate with 4 layers. Actuator case.

	$a\,/\,h$	2	4	10	100	
Ref.[14]	$\boldsymbol{\sigma_{xx}}$	$LD4_a$	3.8162	1.1180	0.1680	-0.0246
	$\boldsymbol{\sigma_{xz}}$	$LD4_a$	0.0864	0.0239	0.0020	0.0000
	$\boldsymbol{\sigma_{xx}}$	LD4	3.8404	1.1249	0.1693	-0.0246
		LD3	3.8618	1.1262	0.1693	-0.0246
		LD2	3.9439	1.1312	0.1695	-0.0246
		LD1	12.4636	3.3532	0.5272	-0.0210
	$\boldsymbol{\sigma_{xz}}$	LD4	0.0929	0.0241	0.0020	0.0000
		LD3	0.0651	0.0227	0.0020	0.0000
		LD2	0.1824	0.0359	0.0028	0.0000
		LD1	0.0215	0.0029	0.0004	0.0000
	$\boldsymbol{\sigma_{zz}}$	LD4	0.0006	0.0001	0.0000	0.0000
		LD3	0.0271	0.0019	0.0001	0.0000
		LD2	0.0547	0.0045	0.0001	0.0000
		LD1	8.1925	2.1772	0.3540	0.0036

Table 5: Principal stresses $\boldsymbol{\sigma_{xx}}$, $\boldsymbol{\sigma_{zz}}$ evaluated along the thickness at *top* ($z = +h/2$) and shear stress $\boldsymbol{\sigma_{xz}}$ evaluated along the thickness in ($z = 0$). Plate with 4 layers. Actuator case.

	$R\,/\,h$		2	4	10	100
Ref.[43]	$w\,(10^9)$	$LFM4_a$	0.0566	0.3332	4.5483	3016.6
	σ_{zz}	$LFM4_a$	-1.1392	-1.0671	-1.0269	-1.0018
	Φ	$LFM4_a$	0.0153	0.0355	0.0942	0.6513
	$\mathcal{D}_z\,(10^9)$	$LFM4_a$	0.0095	0.0028	-0.1646	-111.76
	$w\,(10^9)$	LD4	0.0566	0.3331	4.5473	3017.2876
	$\sigma_{\alpha\alpha}$	LD4	0.4332 -1.4003	2.3837 -3.3497	17.5910 -17.0300	2055.6587 -316.7597
	$\sigma_{\beta\beta}$	LD4	0.9068 -2.0590	4.9006 -6.5066	35.0550 -38.7790	2567.2803 -2542.8062
	$\sigma_{\alpha\beta}$	LD4	0.0008 -0.0008	0.0039 -0.0040	0.0291 -0.0329	1.3707 -4.0802
	$\sigma_{\alpha z}$	LD4	-0.1084	-0.2644	-0.7242	-5.1421
	$\sigma_{\beta z}$	LD4	0.0046	0.0194	0.0750	0.2104
	σ_{zz}	LD4	-0.0798 -1.1658	-0.0469 -1.0914	0.0317 -1.0992	3.2476 -5.2059
	Φ	LD4	0.0153	0.0356	0.0949	0.6696
	$\mathcal{D}_z\,(10^9)$	LD4	0.0054	-0.0179	-0.2668	-111.1786

Table 6: Transverse normal displacement $\boldsymbol{w}*10^9$, electric potential $\boldsymbol{\Phi}$, shear stresses $\boldsymbol{\sigma_{\alpha z}}$, $\boldsymbol{\sigma_{\beta z}}$ evaluated along the thickness in ($z = 0$). Transverse normal electric displacement $\boldsymbol{\mathcal{D}_z} * 10^9$ evaluated along the thickness at *top* ($z = +h/2$). In-plane stresses $\boldsymbol{\sigma_{\alpha\alpha}}$, $\boldsymbol{\sigma_{\beta\beta}}$, $\boldsymbol{\sigma_{\alpha\beta}}$ and transverse normal stress $\boldsymbol{\sigma_{zz}}$ evaluated along the thickness at ($z = \pm h/2$). Shell mono-layered piezoelectric cylinder. $Mesh\,(10\times10)$. Sensor case.

	$R\,/\,h$		2	4	10	100
Ref.[43]	$w\,(10^{11})$	$LFM4_a$	-9.6220	-11.285	6.4540	11277
	σ_{zz}	$LFM4_a$	0.0431	0.0114	0.0004	-0.0001
	Φ	$LFM4_a$	0.3431	0.4611	0.5037	0.5254
	$\mathcal{D}_z\,(10^{11})$	$LFM4_a$	-584.80	-783.99	-1615.6	-16266
	$w\,(10^{11})$	LD4	-9.6219	-11.2852	6.4451	11275.3779
	$\sigma_{\alpha\alpha}$	LD4	-3.2642 -0.9616	-4.4933 -3.5544	-8.9704 -10.3507	-18.4390 -106.9489
	$\sigma_{\beta\beta}$	LD4	0.3518 0.4177	0.3624 0.0395	1.3358 -1.4200	94.4157 -94.1954
	$\sigma_{\alpha\beta}$	LD4	0.0036 0.0005	0.0042 0.0019	0.0082 0.0054	0.1075 -0.0114
	$\sigma_{\alpha z}$	LD4	-0.0207	-0.0207	-0.0324	-0.1905
	$\sigma_{\beta z}$	LD4	0.0023	0.0027	0.0014	0.0072
	σ_{zz}	LD4	0.0731 0.1009	0.0311 0.0371	0.0090 0.0047	0.1865 0.0454
	Φ	LD4	0.3432	0.4611	0.5037	0.5259
	$\mathcal{D}_z\,(10^{11})$	LD4	-586.0881	-786.2541	-1621.7268	-16310.8350

Table 7: Transverse normal displacement $\boldsymbol{w} * 10^{11}$, electric potential $\boldsymbol{\Phi}$, shear stresses $\boldsymbol{\sigma_{\alpha z}}$, $\boldsymbol{\sigma_{\beta z}}$ evaluated along the thickness in $(z = 0)$. Transverse normal electric displacement $\boldsymbol{\mathcal{D}_z} * 10^{11}$ evaluated along the thickness at *top* $(z = +h/2)$. In-plane stresses $\boldsymbol{\sigma_{\alpha\alpha}}$, $\boldsymbol{\sigma_{\beta\beta}}$, $\boldsymbol{\sigma_{\alpha\beta}}$ and transverse normal stress $\boldsymbol{\sigma_{zz}}$ evaluated along the thickness at $(z = \pm h/2)$. Shell mono-layered piezoelectric cylinder. $Mesh\,(10\times10)$. Actuator case.

$R\,/\,h$		2	4	10	100
$w\,(10^{11})$	$LFM4_a$	30.225	111.91	969.70	403190
$\sigma_{\alpha z}$	$LFM4_a$	-0.1193	-0.2575	-0.6365	-3.1560
σ_{zz}	$LFM4_a$	-0.415	-0.661	-1.150	-3.997
Φ	$LFM4_a$	0.00497	0.0195	0.0602	0.3127
$\mathcal{D}_z\,(10^{11})$	$LFM4_a$	0.752	1.104	1.325	-5.495
$w\,(10^{11})$	LD4	30.223	111.906	969.672	403287
	LD1	31.60	111.731	947.779	397293
$\sigma_{\alpha z}$	LD4	-0.1195	-0.2579	-0.6385	-3.2162
	LD1	-0.1144	-0.2383	-0.5845	-2.9859
σ_{zz}	LD4	-0.4129	-0.6597	-1.1529	-4.0875
	LD1	-0.4033	-0.6466	-1.1245	-3.9824
Φ	LD4	0.0050	0.0195	0.0604	0.3190
	LD1	0.0072	0.0212	0.0604	0.3143
$\mathcal{D}_z\,(10^{11})$	LD4	0.1516	-0.8323	-3.0984	-23.473
	LD1	-2.950	-8.7942	-36.282	-1648.83

Table 8: Transverse normal displacement $\boldsymbol{w}*10^{11}$, electric potential $\boldsymbol{\Phi}$, shear stresse $\boldsymbol{\sigma_{\alpha z}}$ and transverse normal stress $\boldsymbol{\sigma_{zz}}$ evaluated along the thickness in $(z = 0)$. Transverse normal electric displacement $\boldsymbol{\mathcal{D}_z} * 10^{11}$ evaluated along the thickness at *top* $(z = +h/2)$. Shell cylinder with 3 layers. Sensor case.

$R\,/\,h$		2	4	10	100
$w\,(10^{11})$	$LFM4_a$	-1.306	-1.400	-1.4667	5.5418
$\sigma_{\alpha z}\,(10^{4})$	$LFM4_a$	19.176	8.4776	1.5865	-0.5423
$\sigma_{zz}\,(10^{4})$	$LFM4_a$	-116.36	-17.086	-0.5748	-0.5571
Φ	$LFM4_a$	0.4058	0.4826	0.5029	0.5009
$\mathcal{D}_z\,(10^{11})$	$LFM4_a$	-106.61	-66.035	-32.684	-36.209
$w\,(10^{11})$	LD4	-1.3066	-1.4007	-1.4662	5.5418
	LD1	-1.3646	-1.4450	-1.4849	5.4331
$\sigma_{\alpha z}\,(10^{4})$	LD4	19.250	8.5036	1.5412	-0.5538
	LD1	11.005	5.5673	0.9585	-0.5193
$\sigma_{zz}\,(10^{4})$	LD4	-119.606	-18.605	3.309	-0.357
	LD1	-82.662	-8.323	5.147	-0.490
Φ	LD4	0.4058	0.4827	0.5029	0.5009
	LD1	0.4917	0.4975	0.4996	0.500
$\mathcal{D}_z\,(10^{11})$	LD4	-106.851	-66.045	-32.642	-36.201
	LD1	-62.002	-38.432	-19.998	-34.863

Table 9: Transverse normal displacement $\boldsymbol{w} * 10^{11}$, electric potential $\boldsymbol{\Phi}$, shear stresse $\boldsymbol{\sigma_{\alpha z}} * 10^{4}$ and transverse normal stress $\boldsymbol{\sigma_{zz}} * 10^{4}$ evaluated along the thickness in $(z = 0)$. Transverse normal electric displacement $\boldsymbol{\mathcal{D}_z} * 10^{11}$ evaluated along the thickness at *top* $(z = +h/2)$. Shell cylinder with 3 layers. Actuator case.

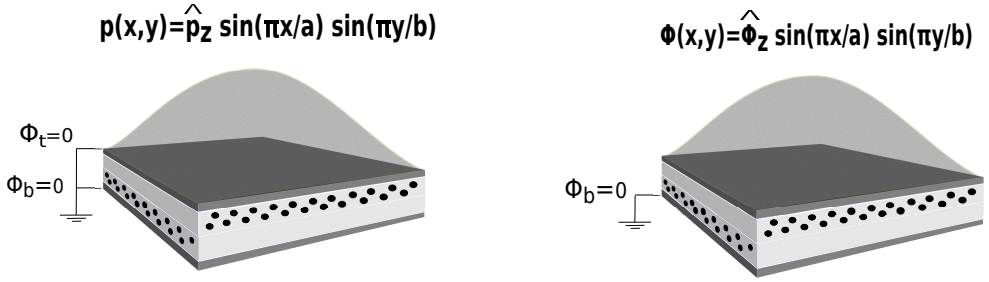

Figure 1: Piezo plate sensor and actuator cases

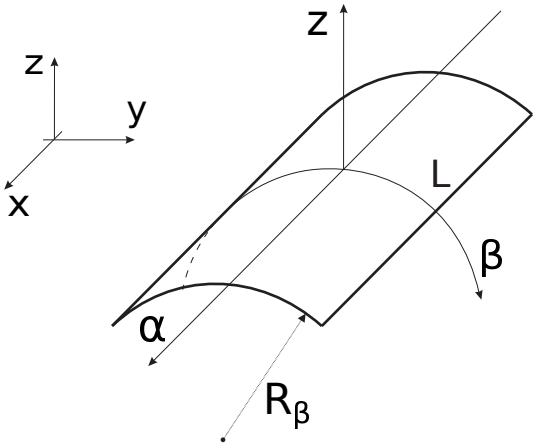

Figure 2: Geometry of the shell.

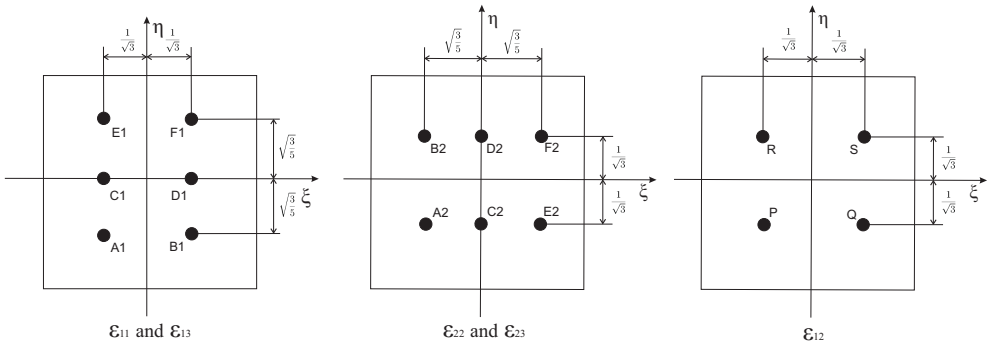

Figure 3: Tying points for the MITC9 shell finite element.

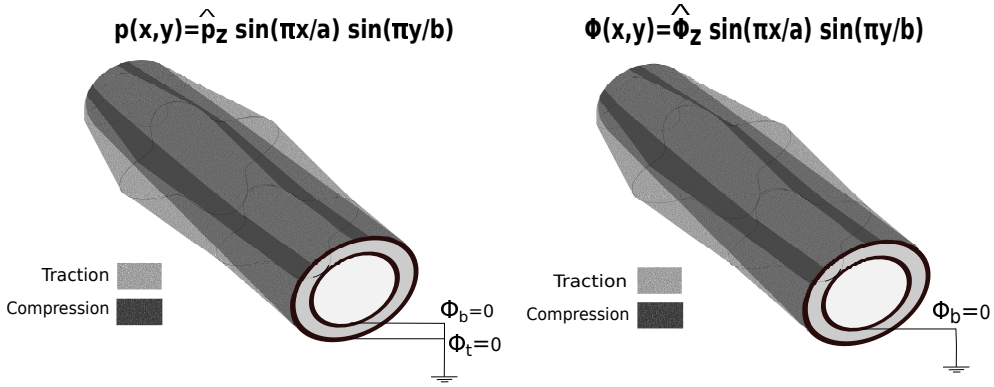

Figure 4: Cylindrical piezo shell, sensor and actuator cases .

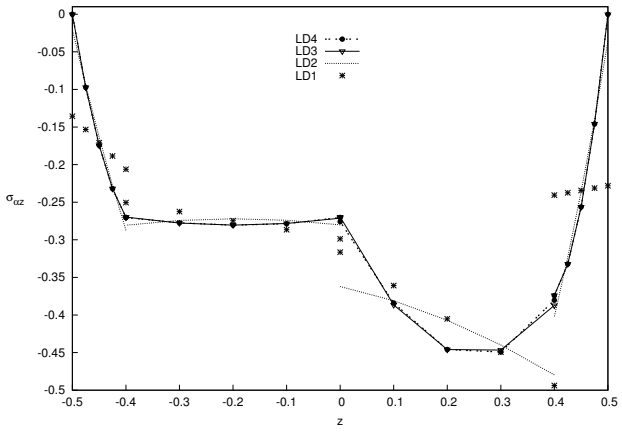

Figure 5: Shear stress $\boldsymbol{\sigma_{\alpha z}}$ along the thickness, with thickness ratio $(a/h) = 2$. Plate with 4 layers. Sensor case.

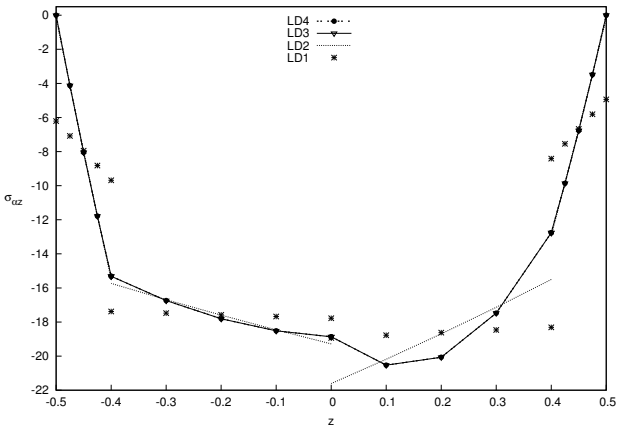

Figure 6: Shear stress $\boldsymbol{\sigma_{\alpha z}}$ along the thickness, with thickness ratio $(a/h) = 100$. Plate with 4 layers. Sensor case.

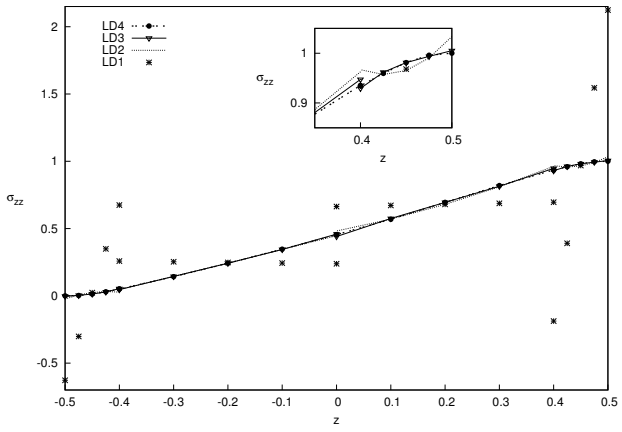

Figure 7: Transverse stress $\boldsymbol{\sigma_{zz}}$ along the thickness, with thickness ratio $(a/h) = 2$. Plate with 4 layers. Sensor case.

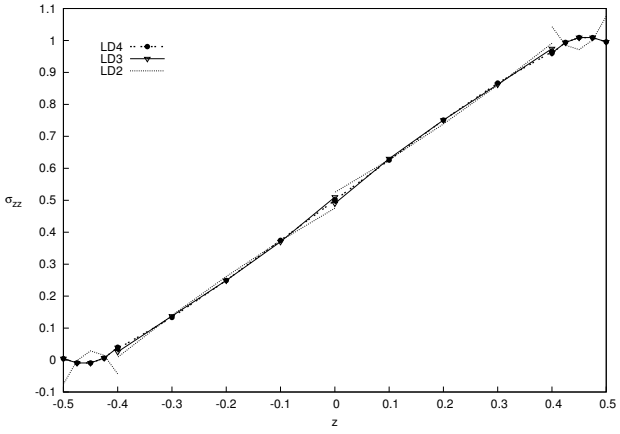

Figure 8: Transverse stress $\boldsymbol{\sigma_{zz}}$ along the thickness, with thickness ratio $(a/h) = 100$. Plate with 4 layers. Sensor case.

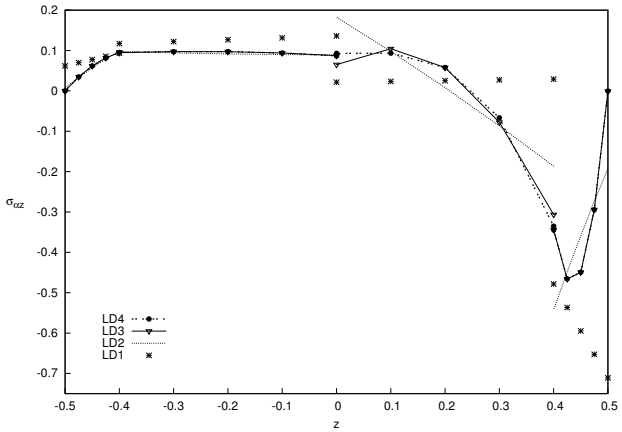

Figure 9: Shear stress $\boldsymbol{\sigma_{\alpha z}}$ along the thickness, with thickness ratio $(a/h) = 2$. Plate with 4 layers. Actuator case.

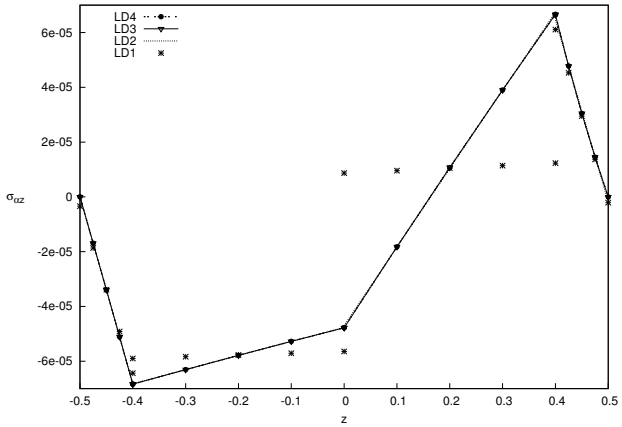

Figure 10: Shear stress $\boldsymbol{\sigma_{\alpha z}}$ along the thickness, with thickness ratio $(a/h) = 100$. Plate with 4 layers. Actuator case.

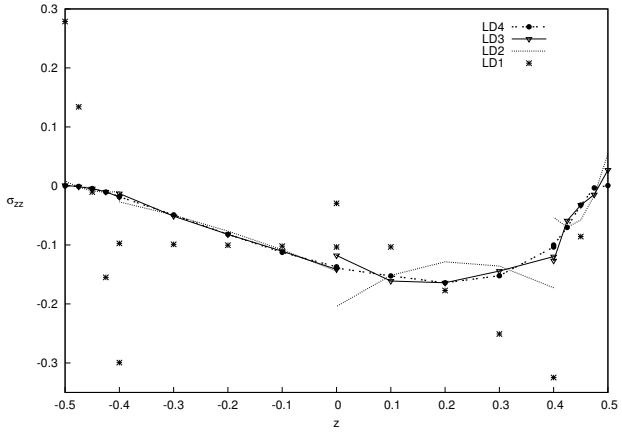

Figure 11: Transverse stress $\boldsymbol{\sigma_{zz}}$ along the thickness, with thickness ratio $(a/h) = 2$. Plate with 4 layers. Actuator case.

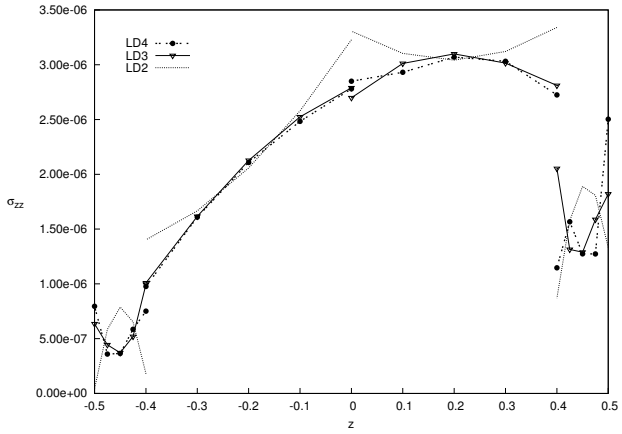

Figure 12: Transverse stress $\boldsymbol{\sigma_{zz}}$ along the thickness, with thickness ratio $(a/h) = 100$. Plate with 4 layers. Actuator case.

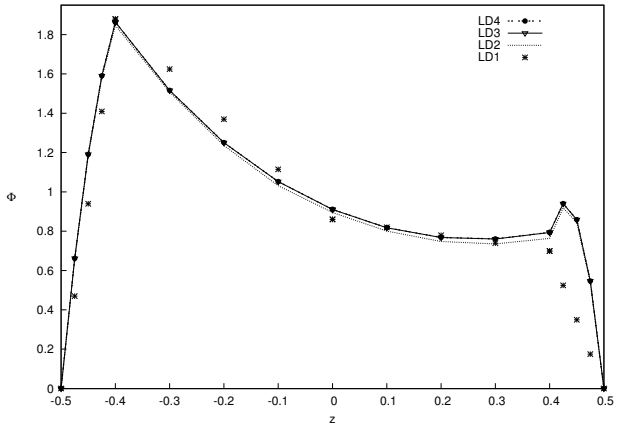

Figure 13: Electric Potential $\mathbf{\Phi}$ along the thickness, with thickness ratio $(a/h) = 2$. Plate with 4 layers. Sensor case.

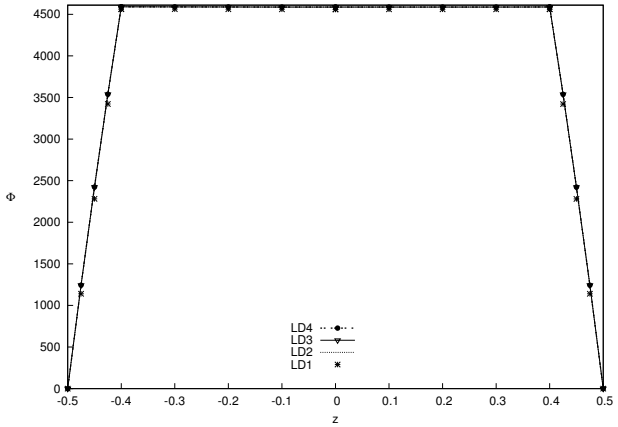

Figure 14: Electric Potential $\mathbf{\Phi}$ along the thickness, with thickness ratio $(a/h) = 100$. Plate with 4 layers. Sensor case.

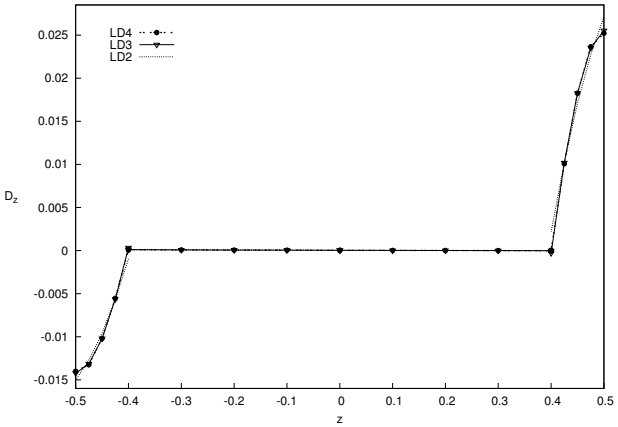

Figure 15: Electric Displacement $\boldsymbol{\mathcal{D}_z}$ along the thickness, with thickness ratio $(a/h) = 2$. Plate with 4 layers. Sensor case.

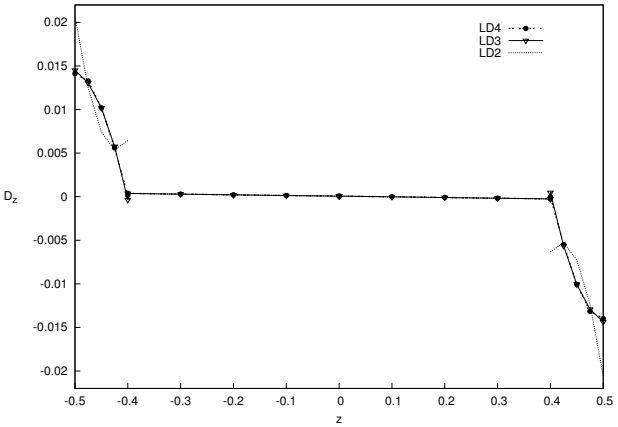

Figure 16: Electric Displacement $\boldsymbol{\mathcal{D}_z}$ along the thickness, with thickness ratio $(a/h) = 100$. Plate with 4 layers. Sensor case.

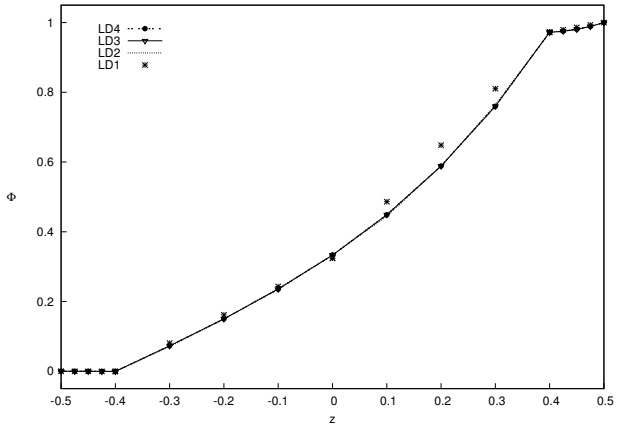

Figure 17: Electric Potential $\mathbf{\Phi}$ along the thickness, with thickness ratio $(a/h) = 2$. Plate with 4 layers. Actuator case.

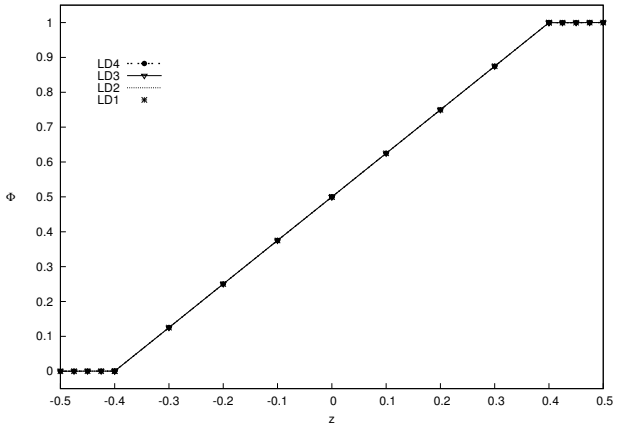

Figure 18: Electric Potential $\mathbf{\Phi}$ along the thickness, with thickness ratio $(a/h) = 100$. Plate with 4 layers. Actuator case.

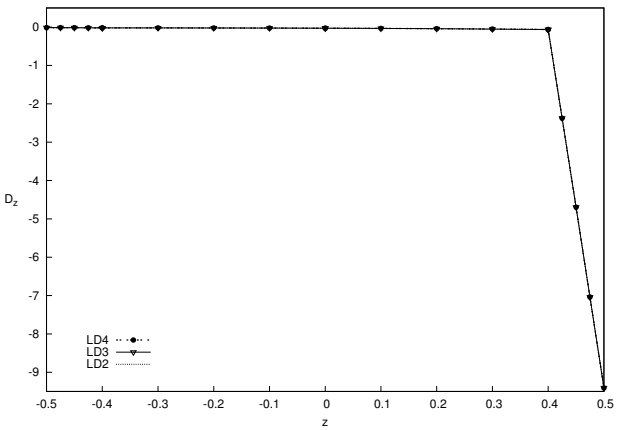

Figure 19: Electric Displacement $\boldsymbol{\mathcal{D}_z}$ along the thickness, with thickness ratio $(a/h) = 2$. Plate with 4 layers. Actuator case.

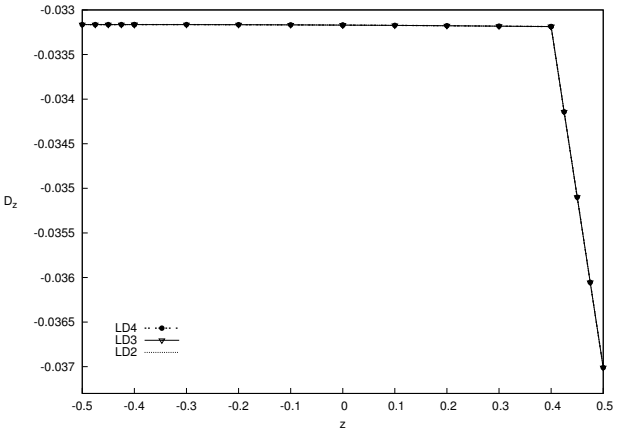

Figure 20: Electric Displacement $\boldsymbol{\mathcal{D}_z}$ along the thickness, with thickness ratio $(a/h) = 100$. Plate with 4 layers. Actuator case.

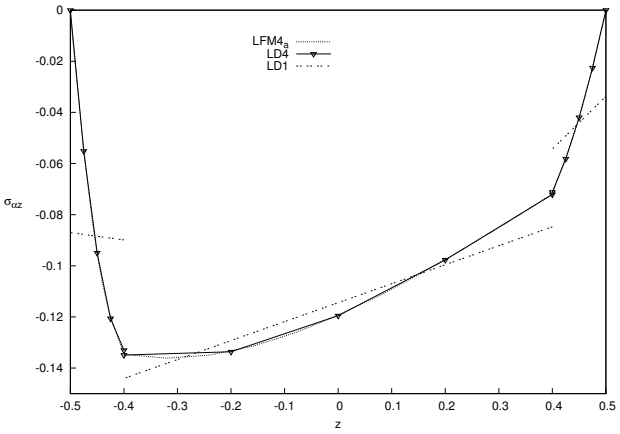

Figure 21: Shear stress $\boldsymbol{\sigma_{\alpha z}}$ along the thickness, with thickness ratio $(R/h) = 2$. Shell with 3 layers. Sensor case.

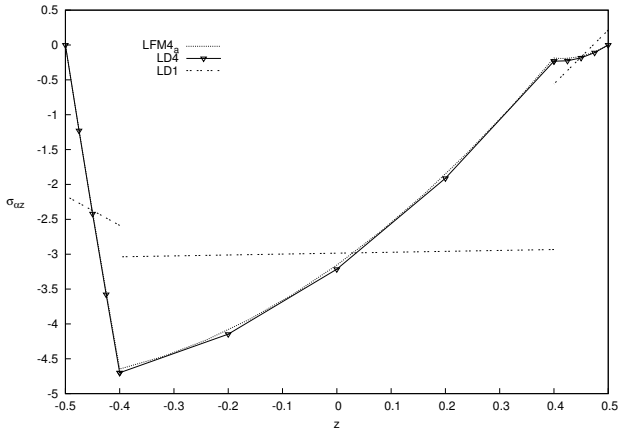

Figure 22: Shear stress $\boldsymbol{\sigma_{\alpha z}}$ along the thickness, with thickness ratio $(R/h) = 100$. Shell with 3 layers. Sensor case.

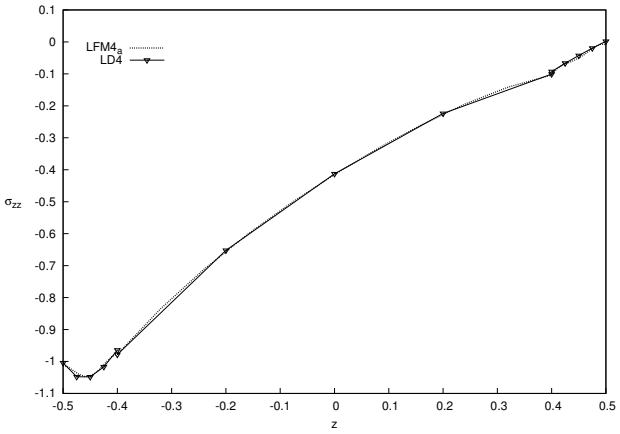

Figure 23: Transverse stress $\boldsymbol{\sigma_{zz}}$ along the thickness, with thickness ratio $(R/h) = 2$. Shell with 3 layers. Sensor case.

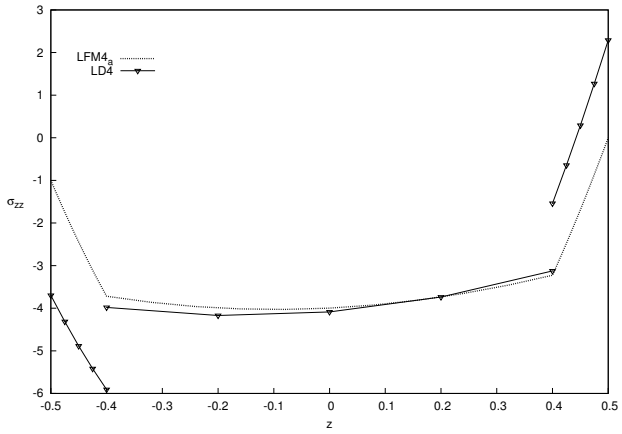

Figure 24: Transverse stress $\boldsymbol{\sigma_{zz}}$ along the thickness, with thickness ratio $(R/h) = 100$. Shell with 3 layers. Sensor case.

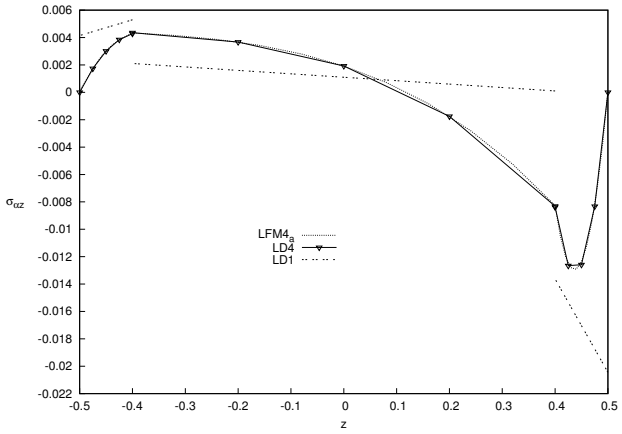

Figure 25: Shear stress $\boldsymbol{\sigma_{\alpha z}}$ along the thickness, with thickness ratio $(R/h) = 2$. Shell with 3 layers. Actuator case.

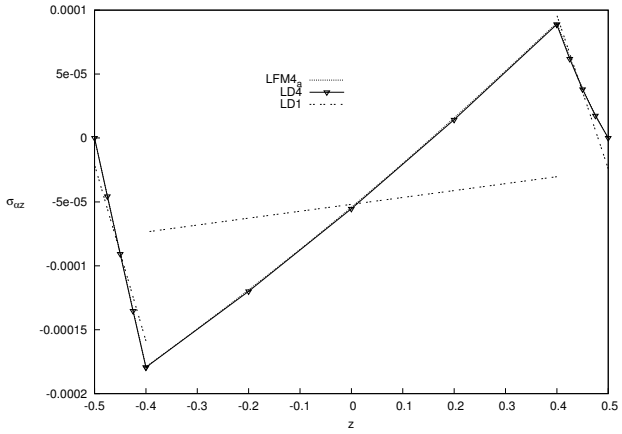

Figure 26: Shear stress $\boldsymbol{\sigma_{\alpha z}}$ along the thickness, with thickness ratio $(R/h) = 100$. Shell with 3 layers. Actuator case.

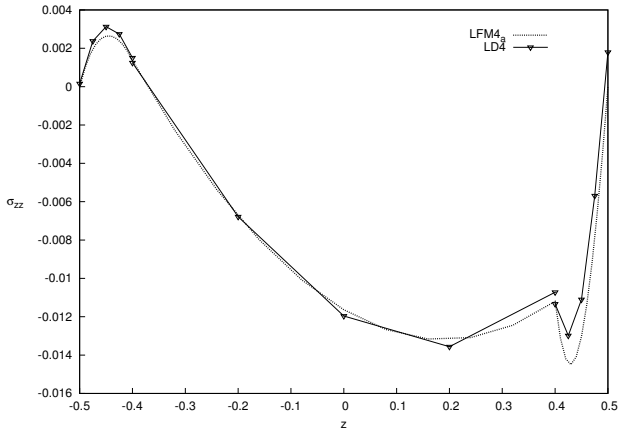

Figure 27: Transverse stress $\boldsymbol{\sigma_{zz}}$ along the thickness, with thickness ratio $(R/h) = 2$. Shell with 3 layers. Actuator case.

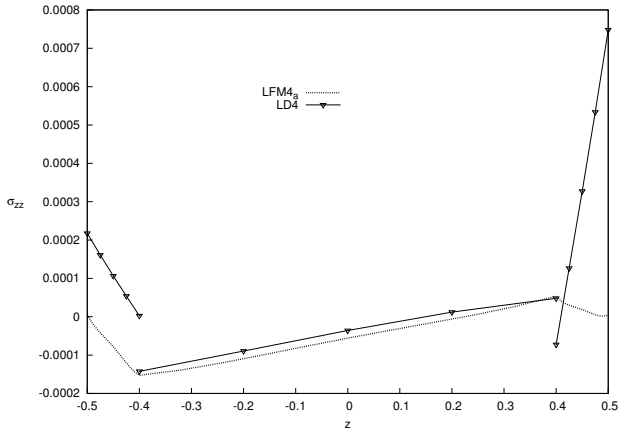

Figure 28: Transverse stress $\boldsymbol{\sigma_{zz}}$ along the thickness, with thickness ratio $(R/h) = 100$. Shell with 3 layers. Actuator case.

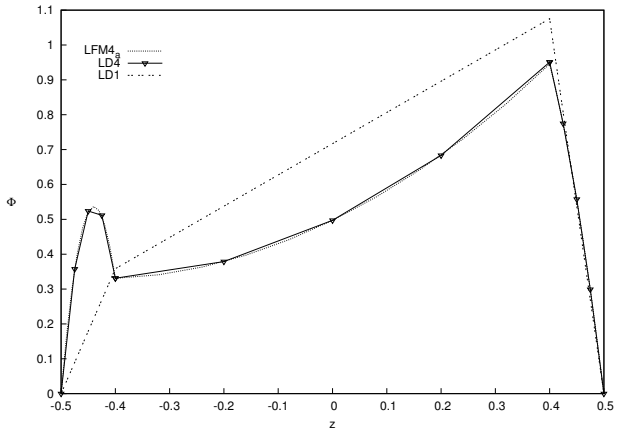

Figure 29: Electric Potential $\mathbf{\Phi}$ along the thickness, with thickness ratio $(R/h) = 2$. Shell with 3 layers. Sensor case.

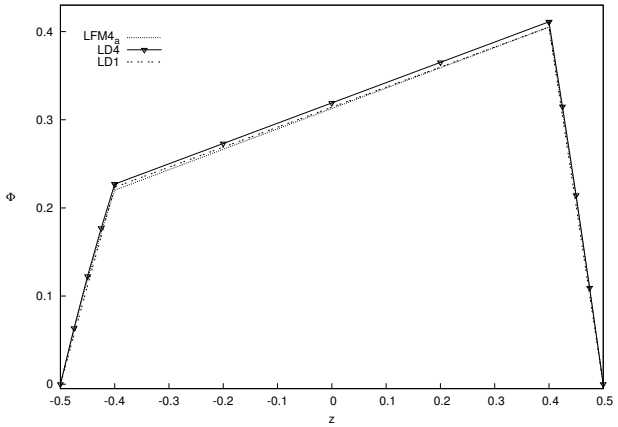

Figure 30: Electric Potential $\mathbf{\Phi}$ along the thickness, with thickness ratio $(R/h) = 100$. Shell with 3 layers. Sensor case.

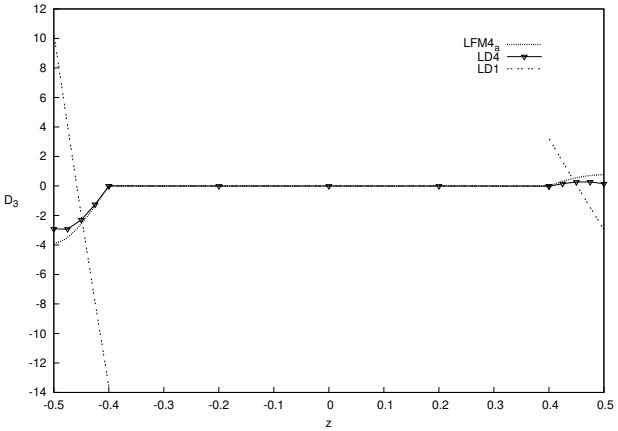

Figure 31: Electric Displacement $\boldsymbol{\mathcal{D}_z}$ along the thickness, with thickness ratio $(R/h) = 2$. Shell with 3 layers. Sensor case.

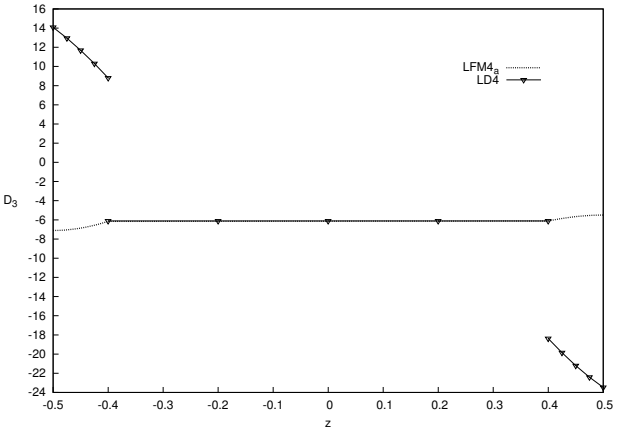

Figure 32: Electric Displacement $\boldsymbol{\mathcal{D}_z}$ along the thickness, with thickness ratio $(R/h) = 100$. Shell with 3 layers. Sensor case.

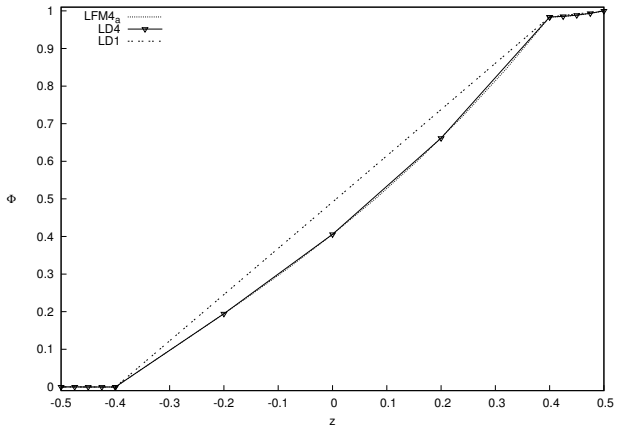

Figure 33: Electric Potential $\mathbf{\Phi}$ along the thickness, with thickness ratio $(R/h) = 2$. Shell with 3 layers. Actuator case.

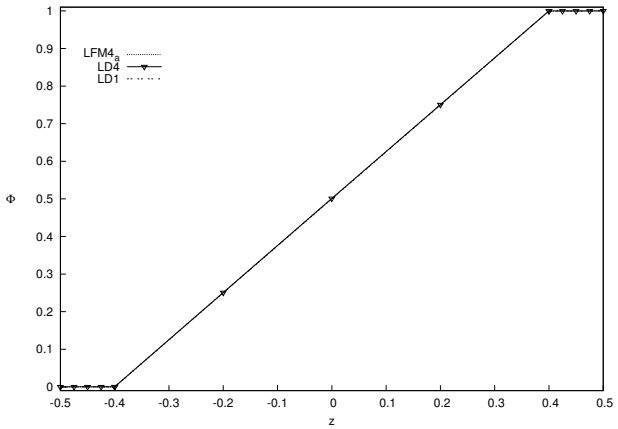

Figure 34: Electric Potential $\mathbf{\Phi}$ along the thickness, with thickness ratio $(R/h) = 100$. Shell with 3 layers. Actuator case.

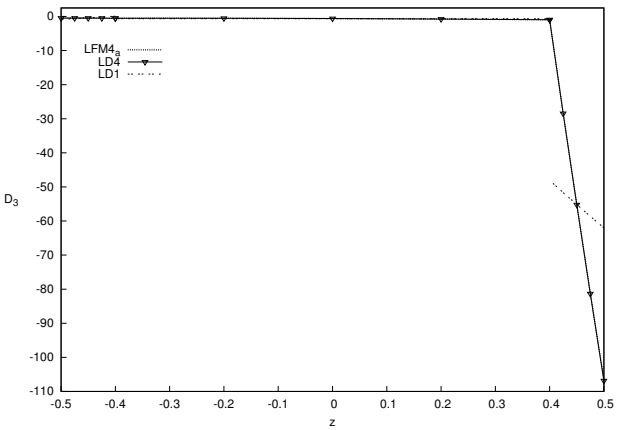

Figure 35: Electric Displacement $\boldsymbol{\mathcal{D}_z}$ along the thickness, with thickness ratio $(R/h) = 2$. Shell with 3 layers. Actuator case.

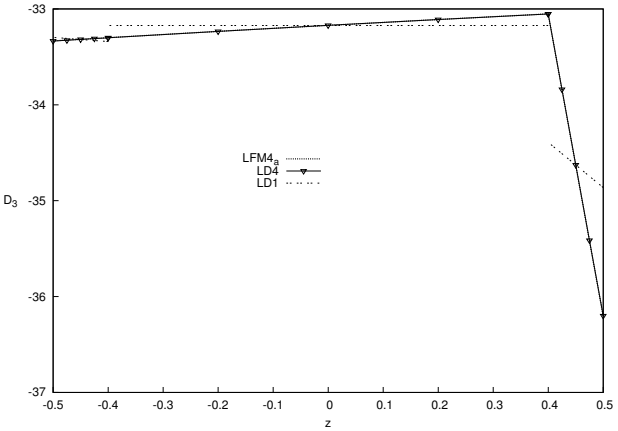

Figure 36: Electric Displacement $\boldsymbol{\mathcal{D}_z}$ along the thickness, with thickness ratio $(R/h) = 100$. Shell with 3 layers. Actuator case.